Magnetic Bloch theorem and reentrant flat bands in twisted bilayer graphene at math xmlns="http://www.w3.org/1998/Math/MathML">mrow>mn>2/mn>mi>π/mi>/mrow>/math> flux

Jonah Herzog-Arbeitman, Aaron Chew, and B. Andrei Bernevig

Phys. Rev. B **106**, 085140 — Published 29 August 2022

DOI: 10.1103/PhysRevB.106.085140

Magnetic Bloch Theorem and Reentrant Flat Bands in Twisted Bilayer Graphene at 2π Flux

Jonah Herzog-Arbeitman[1], Aaron Chew[1], and B. Andrei Bernevig[1,2,3]
[1]*Department of Physics, Princeton University, Princeton, NJ 08544*
[2]*Donostia International Physics Center, P. Manuel de Lardizabal 4, 20018 Donostia-San Sebastian, Spain and*
[3]*IKERBASQUE, Basque Foundation for Science, Bilbao, Spain*
(Dated: August 18, 2022)

Bloch's theorem is the centerpiece of topological band theory, which itself has defined an era of quantum materials research. However, Bloch's theorem is broken by a perpendicular magnetic field, making it difficult to study topological systems in strong flux. For the first time, moiré materials have made this problem experimentally relevant, and its solution is the focus of this work. We construct gauge-invariant irreps of the magnetic translation group at 2π flux on infinite boundary conditions, allowing us to give analytical expressions in terms of the Siegel theta function for the magnetic Bloch Hamiltonian, non-Abelian Wilson loop, and many-body form factors. We illustrate our formalism using a simple square lattice model and the Bistritzer-MacDonald Hamiltonian of twisted bilayer graphene, obtaining reentrant ground states at 2π flux under the Coulomb interaction.

I. INTRODUCTION

Motivated by developments in the fabrication of moiré materials with greatly enlarged unit cells[1–8], this work revisits the solution of continuum Hamiltonians in strong flux from the modern perspective of topological band theory. The essential difficulty of the problem was identified by Zak who demonstrated that translations do not commute in generic magnetic flux and instead form a projective representation of the translation group[9]. As such, Bloch's theorem does not apply. The result is a fractal energy spectrum as a function of magnetic flux known as the Hofstadter butterfly[10–13]. In this work, we present a new formalism to obtain the exact band structure and topology of a continuum Hamiltonian when the flux through a single unit cell is 2π. At 2π flux, corresponding to $\sim$ 25T in magic angle twisted bilayer graphene (TBG)[14], the magnetic translation group commutes due to the Aharonov-Bohm effect, allowing reentrant Hofstadter phases[9,10]. Although methods already exist to study the spectrum in arbitrary magnetic fields[15–30], they are unsuitable for determining the topology and dominant many-body effects essential to moiré physics. Our formalism is manifestly gauge-invariant, leading to analytical expressions for the magnetic Bloch Hamiltonian, non-Abelian Berry connection, and many-body form factors. Importantly, numerical implementation is also straightforward, and we are able to study reentrant phases, which have recently become of interest[31,32], without using simplified models. The methods detailed here were used to study reentrant correlated insulators[33] in twisted bilayer graphene, which have been observed in experiment[34].

We begin with a general discussion of the symmetry operators in Sec. II which are used to construct gauge-invariant magnetic translation group irreps on infinite boundary conditions in Sec. III. A discussion of the Siegel theta function[35–37], a multi-dimensional generalization of the Jacobi theta function which appears in our states, may be found in Ref.[38]. We provide a general expression for the magnetic Bloch Hamiltonian in Sec. IV and compute the band structure for a square lattice model. Then in Sec. V, we define the Berry connection which receives two new magnetic contributions (Abelian and non-Abelian), and we discuss the topological transition between the strong flux or Landau level regime where the kinetic energy dominates and the crystalline regime where the potential dominates. In Sec. VII, we give convenient expressions for the form factors of generic density-density interactions. Finally in Secs. VIII and IX, we study the Bistritzer-MacDonald (BM) Hamiltonian[14] of twisted bilayer graphene which reaches 2π flux at $\sim$ 25T. We discuss the symmetries of TBG at 2π and find that the degree of particle-hole breaking strongly determines the topology of the flat bands, which realize a decomposable elementary band representation[39].

We note that the Hofstadter spectrum of tight-binding models under the Peierls substitution[40] is periodic in flux with the period equal to an integer multiple of 2π depending on the orbitals[41]. This is because gauge fields on the lattice are compact. Such systems differ from the continuum models considered here where there is no exact periodicity in ϕ (though see Ref.[42] for a discussion of approximate periodicity) and we are not reliant on the validity of the Peierls approximation. Notably, the spectrum and topology of the BM model we obtain at 2π flux compares well to tight-binding calculations of twisted bilayer graphene at a small commensurate angle[43].

II. SYMMETRY ALGEBRA

We consider a two-dimensional Hamiltonian minimally coupled to a background gauge field $\mathbf{A}(\mathbf{r})$ in the form

$$H = h(-i\boldsymbol{\nabla} - e\mathbf{A}) + U(\mathbf{r}), \qquad \boldsymbol{\nabla}\times\mathbf{A} = B > 0 \quad (1)$$

where we study $h(p) = p^2/2m$ and $h(p) = v_F(p_x\sigma_x + p_y\sigma_y)$ and set $\hbar = 1$. Here $e > 0$ is the electron charge, the magnetic field B is perpendicular to the plane, and

the cross product is a scalar in two dimensions. We neglect the Zeeman coupling, but it is trivial to add. The potential $U(\mathbf{r})$ is periodic: $U(\mathbf{r}) = U(\mathbf{r}+\mathbf{R})$ where $\mathbf{R}$ is on the Bravais lattice with basis vectors $\mathbf{a}_1, \mathbf{a}_2$ oriented so $\mathbf{a}_1 \times \mathbf{a}_2 = \Omega > 0$.[44] The reciprocal lattice is spanned by the vectors $2\pi\mathbf{b}_i$ satisfying $\mathbf{a}_i \cdot \mathbf{b}_j = \delta_{ij}$. The magnetic flux is $\phi = eB\Omega$ which is dimensionless (setting $\hbar = 1$).

In absence of a periodic potential, the Hamiltonian $h(p)$ in flux can be solved in terms of Landau levels by introducing an oscillator algebra. The algebra is formed from the canonical momentum $\boldsymbol{\pi} = -i\boldsymbol{\nabla} - e\mathbf{A}$ obeying

$$[\pi_\mu, \pi_\nu] = ie(\partial_\mu A_\nu - \partial_\nu A_\mu) = ieB\epsilon_{\mu\nu} \tag{2}$$

where throughout this section, greek letters correspond to cartesian indices, e.g. $\mu, \nu \in \{x, y\}$, and we sum over repeated indices. We define the ladder operators $[a, a^\dagger] = 1$ by

$$a = \frac{\pi_x + i\pi_y}{\sqrt{2eB}}, a^\dagger = \frac{\pi_x - i\pi_y}{\sqrt{2eB}} \ . \tag{3}$$

In the simplest case of $h(p) = p^2/2m = eB(a^\dagger a + 1/2)$ in magnetic field, the eigenstates are Landau levels given by powers of $a^\dagger$. The macroscopic degeneracy of the Landau levels is accounted for by the guiding center momenta Q_μ. The gauge-invariant definition is

$$Q_\mu = \pi_\mu - eB\epsilon_{\mu\nu}x_\nu = -i\partial_\mu - e(A_\mu + B\epsilon_{\mu\nu}x_\nu) \ . \tag{4}$$

The guiding center operators commute with the canonical momenta and obey

$$\begin{aligned}[Q_\mu, \pi_\nu] &= [\pi_\mu - eB\epsilon_{\mu\rho}x_\rho, \pi_\nu] = ieB\epsilon_{\mu\nu} - ieB\epsilon_{\mu\nu} = 0 \\ [Q_\mu, Q_\nu] &= [\pi_\mu - eB\epsilon_{\mu\rho}x_\rho, \pi_\nu - eB\epsilon_{\nu\sigma}x_\sigma] = -ieB\epsilon_{\mu\nu} \ .\end{aligned} \tag{5}$$

The guiding centers form a separate oscillator system with $[b, b^\dagger] = 1$ defined by (see Ref.[38])

$$b = \frac{(\mathbf{a}_1 - i\mathbf{a}_2)\cdot\mathbf{Q}}{\sqrt{2\phi}}, \quad b^\dagger = \frac{(\mathbf{a}_1 + i\mathbf{a}_2)\cdot\mathbf{Q}}{\sqrt{2\phi}}, \tag{6}$$

Note that the b-oscillators commute with the a-oscillators by Eq. (5). Comparing Eq. (6) and Eq. (3), we see that the $a, a^\dagger$ operators are defined using cartesian variables while the $b, b^\dagger$ operators are defined using the lattice vectors. This is because the $a, a^\dagger$ operators are used to build the continuum kinetic term which has $SO(2)$ rotation symmetry, while the $b, b^\dagger$ operators will be used to construct states that respect the lattice periodicity.

The kinetic term $h(\boldsymbol{\pi})$, which is built out of a and $a^\dagger$ operators, commutes with $b, b^\dagger$. Hence without a potential, every Landau level eigenstate has an infinite degeneracy (on infinite boundary conditions) from acting repeatedly with $b^\dagger$ because $[h(\boldsymbol{\pi}), \mathbf{Q}] = 0$. A periodic potential breaks this degeneracy. However, we observe that the magnetic translation operators

$$T_{\mathbf{a}_i} = \exp\left(i\mathbf{a}_i \cdot \mathbf{Q}\right) \tag{7}$$

formed from the Q_i algebra commute with a periodic potential. Using the Baker-Campbell-Hausdorff (BCH) formula, we check

$$\begin{aligned}e^{i\mathbf{a}_i\cdot\mathbf{Q}}U(\mathbf{r})e^{-i\mathbf{a}_i\cdot\mathbf{Q}} &= \sum_{n=0}^{\infty}\frac{1}{n!}\Big([i\mathbf{a}_i\cdot\mathbf{Q},\Big)^n U(\mathbf{r})] \\ &= \sum_{n=0}^{\infty}\frac{1}{n!}\big([i\mathbf{a}_i\cdot(-i\boldsymbol{\nabla}),\big)^n U(\mathbf{r})] \\ &= e^{\mathbf{a}_i\cdot\boldsymbol{\nabla}}U(\mathbf{r})e^{-\mathbf{a}_i\cdot\boldsymbol{\nabla}} \\ &= U(\mathbf{r}+\mathbf{a}_i) = U(\mathbf{r}) \ .\end{aligned} \tag{8}$$

where the nested commutator $([X,)^n Y] = [X, [X, \ldots, Y]]$ has n factors of X and in the last line we used the lattice periodicity. This is sufficient to prove that $T_{\mathbf{a}_i}$ commutes with the whole Hamiltonian H (kinetic plus potential) because $[\mathbf{Q}, \boldsymbol{\pi}] = 0$ and the kinetic term only contains $\boldsymbol{\pi}$ operators. Note that $[H, \mathbf{Q}] \neq 0$ but $[H, e^{i\mathbf{a}_i\cdot\mathbf{Q}}] = 0$ for a periodic potential. The algebra of the $T_{\mathbf{a}_i}$ operators is derived from the BCH formula by

$$T_{\mathbf{a}_1}T_{\mathbf{a}_2} = \exp\Big([i\mathbf{a}_1\cdot\mathbf{Q}, i\mathbf{a}_2\cdot\mathbf{Q}]\Big)T_{\mathbf{a}_2}T_{\mathbf{a}_1} = e^{i\phi}T_{\mathbf{a}_2}T_{\mathbf{a}_1} \ . \tag{9}$$

Eq. (9) shows that the magnetic translation operators define a projective representation of the translation group. For generic $\phi \in \mathbb{R}$, $T_{\mathbf{a}_1}$ and $T_{\mathbf{a}_2}$ do not commute and there is no band structure. The cascade of band splitting that occurs as the flux is increased leads to the fractal Hofstadter energy spectrum[10]. The $a^\dagger$ and $b^\dagger$ operators form a basis of the Hilbert space which is used to solve continuum Hamiltonians in terms of degenerate Landau levels. In Sec. III, we will produce basis states which are magnetic translation operator irreps by recombining the $b^\dagger$ basis.

So far, the flux $\phi = eB\Omega$ has been unrestricted. In the following sections, we fix $\phi = 2\pi$ where Eq. (9) shows that the magnetic translation operators commute. This is an intrinsically quantum mechanical effect because 2π flux corresponds to one flux quantum h/e piercing each unit cell where h is Planck's constant. In a conventional crystal where the unit cell area is on the order of 10Å^2, $\phi = 2\pi$ corresponds to extreme fields between 10^4T and 10^5T. However, moiré materials have an effective unit cell which is larger by a factor of θ^{-2} where θ is the twist angle. For angles near 1°, the moiré unit cell is enlarged by a factor of 3000 allowing $\sim$ 25T fields to probe the Hofstadter regime.

III. MAGNETIC TRANSLATION GROUP IRREPS

In this section, we construct wavefunctions which are irreps of the magnetic translation group at $\phi = 2\pi$ on infinite boundary conditions in a gauge-invariant manner. These states are the building blocks of all subsequent calculations. To motivate them, we first revisit Bloch's theorem in zero flux.

A. Bloch's Theorem

Let us briefly recall the traditional Bloch theorem. The translation group in zero flux on infinite boundary conditions is isomorphic to the infinite group $\mathbb{Z}^2$ which is Abelian. Hence its irreducible representations (irreps) are all one-dimensional. They are eigenstates of the translation operators labeled by a crystal momentum $\mathbf{k} = k_1\mathbf{b}_1 + k_2\mathbf{b}_2$ where $k_i \in (-\pi, \pi)$ defines the Brillouin zone (BZ). It is trivial to construct the first-quantized eigenstates of the zero-flux translation operators $T_{\mathbf{R}} = e^{\mathbf{R}\cdot\boldsymbol{\nabla}}$ with eigenvalue $e^{i\mathbf{k}\cdot\mathbf{R}}$ where $\mathbf{R} = R_1\mathbf{a}_1 + R_2\mathbf{a}_2,\ R_i \in \mathbb{Z}$: the functions $\psi^{\phi=0}_{\mathbf{k},n}(\mathbf{r}) = e^{i\mathbf{k}\cdot\mathbf{r}}u_{\mathbf{k},n}(\mathbf{r})$ are momentum eigenstates for any periodic function $u_{\mathbf{k},n}(\mathbf{r}) = u_{\mathbf{k},n}(\mathbf{r}+\mathbf{a}_i)$ which we normalize to

$$\int_\Omega d^2x\, u^*_{\mathbf{k},m}(\mathbf{x})u_{\mathbf{k},n}(\mathbf{x}) = \delta_{mn} \tag{10}$$

by integrating over the unit cell Ω. Hence the functions $u^*_{\mathbf{k},m}(\mathbf{x})$ form a complete basis of periodic functions on the unit cell at each $\mathbf{k}$. In this case, the Bloch waves $\psi^{\phi=0}_{\mathbf{k},n}(\mathbf{r})$ normalized on infinite boundary conditions as

$$\begin{aligned}
&\int d^2r\, \psi^{\phi=0}_{\mathbf{k},m}(\mathbf{r})^*\psi^{\phi=0}_{\mathbf{k}',n}(\mathbf{r}) \\
&= \sum_{\mathbf{R}} e^{i(\mathbf{k}'-\mathbf{k})\cdot\mathbf{R}}\int_\Omega d^2x\, e^{i(\mathbf{k}'-\mathbf{k})\cdot\mathbf{x}}u^*_{\mathbf{k},m}(\mathbf{x})u_{\mathbf{k}',n}(\mathbf{x}) \\
&= (2\pi)^2\delta(\mathbf{k}-\mathbf{k}')\int_\Omega d^2x\, u^*_{\mathbf{k},m}(\mathbf{x})u_{\mathbf{k},n}(\mathbf{x}) \\
&= (2\pi)^2\delta_{mn}\delta(\mathbf{k}-\mathbf{k}')
\end{aligned} \tag{11}$$

using the identity $(2\pi)^2\delta(\mathbf{k}-\mathbf{k}') = \sum_{\mathbf{R}} e^{i\mathbf{R}\cdot(\mathbf{k}-\mathbf{k}')}$ with $\mathbf{k}-\mathbf{k}' \in BZ$. The periodic functions $u_{\mathbf{k},n}(\mathbf{r})$ form an orthonormal basis of states within a single unit cell, and can be chosen as the eigenstates of the effective Bloch Hamiltonian $e^{-i\mathbf{k}\cdot\mathbf{r}}He^{i\mathbf{k}\cdot\mathbf{r}}$ which is a function of $\mathbf{k}$. Note that there are an infinite number of eigenstates $u_{\mathbf{k},n}(\mathbf{r})$ because the Hilbert space is infinite dimensional. At each $\mathbf{k} \in BZ$, $n = 1, 2, \ldots$ indexes Bloch waves of increasingly high energy. This contrasts the tight-binding approximation where only a finite number of Bloch waves are kept and the local Hilbert space is finite dimensional.

To parallel our construction at $\phi = 2\pi$ in Sec. III B, we now give an alternative representation for the Bloch waves. We introduce the Wannier functions

$$w^{\phi=0}_{\mathbf{R},n}(\mathbf{r}) \equiv T_{\mathbf{R}}w^{\phi=0}_n(\mathbf{r}) = \int \frac{d^2k}{(2\pi)^2}e^{i\mathbf{k}\cdot(\mathbf{r}+\mathbf{R})}u_{\mathbf{k},n}(\mathbf{r}) \tag{12}$$

which, being formed from states at different $\mathbf{k}$, are generally not energy or momentum eigenstates. Instead the Wannier functions $w^{\phi=0}_{\mathbf{R}n}(\mathbf{r})$ form a local basis of the Hilbert space which is complementary to the entirely delocalized Bloch wave basis (see Ref.[45] for a thorough discussion). A Bloch state can be built from the Wannier functions according to

$$\psi^{\phi=0}_{\mathbf{k},n}(\mathbf{r}) = \sum_{\mathbf{R}} e^{-i\mathbf{k}\cdot\mathbf{R}}T_{\mathbf{R}}w^{\phi=0}_n(\mathbf{r}) \tag{13}$$

which can be proven directly from Eq. (12):

$$\begin{aligned}
\sum_{\mathbf{R}} e^{-i\mathbf{k}\cdot\mathbf{R}}T_{\mathbf{R}}w^{\phi=0}_n(\mathbf{r}) &= \int \frac{d^2k'}{(2\pi)^2}\sum_{\mathbf{R}} e^{i(\mathbf{k}-\mathbf{k}')\cdot\mathbf{R}}e^{i\mathbf{k}'\cdot\mathbf{r}}u_{\mathbf{k}',n}(\mathbf{r}) \\
&= \psi^{\phi=0}_{\mathbf{k},n}(\mathbf{r})
\end{aligned} \tag{14}$$

Note that the construction in Eq. (13) is guaranteed to be a momentum eigenstate (if not an energy eigenstate) for any $w^{\phi=0}_n(\mathbf{r})$, not necessarily a Wannier function. We now make use of this observation to produce magnetic translation group eigenstates at $\phi = 2\pi$.

B. Magnetic Bloch Theorem at $\phi = 2\pi$

At 2π flux, the magnetic translation group commutes (see Eq. (9)) and is isomorphic to $\mathbb{Z}^2$. Hence its irreps are again labeled by $\mathbf{k} = k_1\mathbf{b}_1 + k_2\mathbf{b}_2 \in BZ$ which we refer to as the momentum. This quantum number is essential to determining the topology of the Hamiltonian. This differentiates our approach from the open momentum space diagonalization technique developed in Ref.[28] which does not make use of the momentum, but achieves a sparse matrix representation of the Hamiltonian at all fluxes.

To derive a magnetic Bloch Hamiltonian in each $\mathbf{k}$ sector, we must construct eigenstates $\psi_{\mathbf{k},n}(\mathbf{r})$ of the magnetic translation operators. We will do so on infinite boundary conditions so that $\mathbf{k}$ is continuous. Using the explicit operators in Eq. (7), there is a natural construction by summing over the infinite Bravais lattice $\mathbf{R}$.[46] Noting that $\mathbf{R}\cdot\mathbf{b}_i \in \mathbb{Z}$, we define the states

$$\psi_{\mathbf{k},n}(\mathbf{r}) = \frac{1}{\sqrt{\mathcal{N}(\mathbf{k})}}\sum_{\mathbf{R}} e^{-i\mathbf{k}\cdot\mathbf{R}}T_{\mathbf{a}_1}^{\mathbf{R}\cdot\mathbf{b}_1}T_{\mathbf{a}_2}^{\mathbf{R}\cdot\mathbf{b}_2}w_n(\mathbf{r}) \tag{15}$$

where $w_n(\mathbf{r})$ is a function to be chosen momentarily. Importantly, the states Eq. (15) take the same form in any gauge. It is direct to check that $T_{\mathbf{a}_i}\psi_{\mathbf{k},n}(\mathbf{r}) = e^{i\mathbf{k}\cdot\mathbf{a}_i}\psi_{\mathbf{k},n}(\mathbf{r})$ because $[T_{\mathbf{a}_i}, T_{\mathbf{a}_j}] = 0$ at $\phi = 2\pi$. Hence the states $\psi_{\mathbf{k},n}$ are orthogonal in $\mathbf{k} \in BZ$. Similar states have been constructed for tight-binding models in Ref.[41]. To achieve orthogonality in n, we use the $a, a^\dagger$ operators which commute with $T_{\mathbf{a}_i}$ to define

$$w_n(\mathbf{r}) = \frac{a^{\dagger n}}{\sqrt{n!}}\psi_0(\mathbf{r}), \qquad a\psi_0(\mathbf{r}) = b\psi_0(\mathbf{r}) = 0\ . \tag{16}$$

It follows that the states $\psi_{\mathbf{k},n}(\mathbf{r})$ are orthogonal because they are eigenstates of the Hermitian Landau level operator $a^\dagger a$ with eigenvalue n. We will not need an explicit expression for the Landau level groundstate $\psi_0(\mathbf{r})$, but

one can be obtained because a and b are commuting linear differential operators, so the first order differential equations in Eq. (16) can be directly integrated.[47]

Lastly, the normalization $\mathcal{N}(\mathbf{k})$ in Eq. (15) is defined by requiring

$$\int d^2r\, \psi^\dagger_{\mathbf{k},m}(\mathbf{r})\psi_{\mathbf{k}',n}(\mathbf{r}) = (2\pi)^2\delta(\mathbf{k}-\mathbf{k}')\delta_{mn} \tag{17}$$

which, after a detailed calculation contained in Ref.[38], yields

$$\mathcal{N}(\mathbf{k}) = \vartheta\left(\frac{(k_1,k_2)}{2\pi}\middle|\,\Phi\right), \quad \Phi = \frac{i}{2}\begin{pmatrix}1 & i\\ i & 1\end{pmatrix}. \tag{18}$$

The function $\vartheta(\mathbf{z}|\Phi)$ is called the Siegel theta function.[48] It is a multi-dimensional generalization of the Jacobi theta function defined for $\mathbf{z}\in\mathbb{C}^2$ by

$$\vartheta(\mathbf{z}\,|\Phi) = \sum_{\mathbf{n}\in\mathbb{Z}^2} e^{2\pi i\left(\frac{1}{2}\mathbf{n}\cdot\Phi\cdot\mathbf{n}-\mathbf{z}\cdot\mathbf{n}\right)}. \tag{19}$$

The matrix Φ which defines the Siegel theta function is sometimes called the Riemann matrix. For the sum in Eq. (19) to converge, Im Φ must be a positive definite matrix. In Ref.[38], we show that Φ is a special "self-dual" Riemann matrix which permits the Siegel theta function to be written in terms of Jacobi theta functions at $\phi = 2\pi$. It is apparent from Eq. (19) that $\mathcal{N}(\mathbf{k}+2\pi\mathbf{b}_i) = \mathcal{N}(\mathbf{k})$, which matches the periodicity of the BZ. The Siegel theta function is quasi-periodic for complex $\mathbf{z}$. A self-contained derivation of the quasi-periodicity may be found in Ref.[38]. We show in Ref.[38] that $\mathcal{N}(\mathbf{k})\geq 0$ for $\mathbf{k}\in BZ$ but at $\pi\mathbf{b}_1+\pi\mathbf{b}_2$, $\mathcal{N}(\mathbf{k})$ has a quadratic zero. Thus the states $\psi_{\mathbf{k},n}$ do not exist exactly at $\mathbf{k}^* = \pi\mathbf{b}_1+\pi\mathbf{b}_2$. We show in Ref.[38] that the wavefunction can be defined in patches by shifting the operator $\mathbf{Q}\to\mathbf{Q}+\mathbf{p}$ which shifts the undefined states to $\mathbf{k}^*+\mathbf{p}$. In fact, the existence of a zero is topologically protected because the states $\psi_{\mathbf{k},n}$ carry nonzero Chern number (see Sec. V) and hence cannot be well-defined and periodic everywhere in the BZ. We will show in Sec. IV that the magnetic Bloch Hamiltonian used to compute the spectrum is an analytic function of $\mathbf{k}$, so the zero in $\mathcal{N}(\mathbf{k})$ only introduces a removable singularity in the Hamiltonian. Lastly, we give a gauge-invariant proof in Ref.[38] that the $\psi_{\mathbf{k},n}$ basis is complete when acting on suitable test functions.

For brevity, we now define braket notation for the magnetic translation operator eigenstates Eq. (15):

$$|\mathbf{k},n\rangle \equiv \frac{1}{\sqrt{\mathcal{N}(\mathbf{k})}}\sum_{\mathbf{R}} e^{-i\mathbf{k}\cdot\mathbf{R}}T_{\mathbf{a}_1}^{\mathbf{R}\cdot\mathbf{b}_1}T_{\mathbf{a}_2}^{\mathbf{R}\cdot\mathbf{b}_2}|n\rangle,\ |n\rangle = \frac{a^{\dagger n}}{\sqrt{n!}}|0\rangle, \tag{20}$$

and $a|0\rangle = b|0\rangle = 0$. For Hamiltonians with additional degrees of freedom indexed by α, such as spin, sublattice, valley, or layer (see Sec. VIII), the basis states of the Hamiltonian can be defined $|\mathbf{k},n,\alpha\rangle = |\alpha\rangle\otimes|\mathbf{k},n\rangle$. In braket notation, Eq. (17) reads

$$\langle\mathbf{k},m|\mathbf{k}',n\rangle = (2\pi)^2\delta_{mn}\delta(\mathbf{k}-\mathbf{k}') \tag{21}$$

and it should be implicitly understood that $\mathbf{k} = \pi\mathbf{b}_1+\pi\mathbf{b}_2$ is excluded from the basis. While discussing single-particle physics in Sec. IV and Sec. V, the braket notation is useful for shortening expressions. Lastly, the structure of the states in Eq. (20) generalizes to the q-dimensional irreps of the magnetic translation group at rational flux $\phi = \frac{2\pi p}{q}$. We leave this construction to future work.

Before concluding this section, we will emphasize the difference between our gauge invariant construction and the commonly used Landau gauge states (see e.g. Ref.[16,27,29]). In the Landau gauge $\mathbf{A} = B(0,x)$ which preserves translation along the y direction for instance, a basis of "Landau level states" can be labeled by k_y and a Landau level index n. These states are fully delocalized along y and localized on the scale of the magnetic length in harmonic oscillator wavefunctions along x[29]. To form eigenstates of the magnetic translation group, these states are resummed to obtain magnetic translation invariance along x. This process is somewhat involved and obscures the physical symmetry of the system since it treats x and y differently due to the asymmetry of the Landau gauge. In contrast, our gauge-invariant construction in Eq. (20) is manifestly symmetric under the magnetic translation group and is immediately valid for arbitrary lattices. It has many practical advantages: all calculations can be performed using the oscillator algebra Eq. (5), and the singularity due to the Chern number of the states is made explicit. This latter feature in particular has not been discussed in earlier treatments, and makes it possible for us to apply the tools of topological band theory in direct analogy to the Bloch wave formalism at zero flux.

IV. MATRIX ELEMENTS

Because the Hamiltonian $H^{\phi=2\pi}$ commutes with the magnetic translation group, it must be diagonal in $\mathbf{k}$ because of the selection rule

$$\langle\mathbf{k}',m|H^{\phi=2\pi}|\mathbf{k},n\rangle = e^{i(\mathbf{k}-\mathbf{k}')\cdot\mathbf{a}_i}\langle\mathbf{k}',m|H^{\phi=2\pi}|\mathbf{k},n\rangle \tag{22}$$

which shows that if $k_i - k_i' \neq 0 \mod 2\pi$, then $\langle\mathbf{k}',m|H^{\phi=2\pi}|\mathbf{k},n\rangle = 0$. Eq. (22) follows from inserting $1 = T^\dagger_{\mathbf{a}_i}T_{\mathbf{a}_i}$ and commuting $T_{\mathbf{a}_i}$ through $H^{\phi=2\pi}$. Having constructed a basis of states which is diagonal in $\mathbf{k}$, we define an effective "Bloch" Hamiltonian $H^{\phi=2\pi}_{mn}(\mathbf{k})$ according to

$$(2\pi)^2\delta(\mathbf{k}-\mathbf{k}')H^{\phi=2\pi}_{mn}(\mathbf{k}) = \langle\mathbf{k}',m|H^{\phi=2\pi}|\mathbf{k},n\rangle \tag{23}$$

which can be diagonalized after imposing a Landau level cutoff. To compute the effective Hamiltonian, we need formulas for the matrix elements of Eq. (1). The kinetic term is simple because $h(\boldsymbol{\pi})$ is composed of $a, a^\dagger$ operators, so it only acts on the m,n indices and its matrix elements will not depend on $\mathbf{k}$ (see Sec. VI for an example). Hence we focus on the potential term $U(\mathbf{r})$ which causes scattering between different Landau levels. Recall

that $U(\mathbf{r})$ is periodic so can be expanded as a Fourier series. Hence we need to compute the general scattering amplitude

$$\langle \mathbf{k}, m | e^{-2\pi i \mathbf{G}\cdot\mathbf{r}} | \mathbf{k}, n\rangle , \quad \mathbf{G} = G_1\mathbf{b}_1 + G_2\mathbf{b}_2,\ G_1, G_2 \in \mathbb{Z} . \tag{24}$$

It is possible to perform the calculation exactly without choosing a gauge for $\mathbf{A}(\mathbf{r})$ because $\mathbf{G}\cdot\mathbf{r}$ can be expressed simply in terms of $\boldsymbol{\pi}$ and $\mathbf{Q}$ using

$$(eB)^{-1}\epsilon_{\mu\nu}(Q_\nu - \pi_\nu) = -\epsilon_{\mu\nu}\epsilon_{\nu\rho}x_\rho = x_\mu \tag{25}$$

which allows the us to perform the calculation using BCH. The details may be found in Ref.[38]. The result is

$$\begin{aligned}&\langle \mathbf{k}', m | e^{-2\pi i \mathbf{G}\cdot\mathbf{r}} | \mathbf{k}, n\rangle = \\ &\qquad (2\pi)^2\delta(\mathbf{k}-\mathbf{k}')e^{-i\pi G_1G_2 - i(G_1k_2 - G_2k_1)}\mathcal{H}^{2\pi\mathbf{G}}_{mn}\end{aligned} \tag{26}$$

where we have defined the Landau level scattering matrix for a general momentum $\mathbf{q}$ with $q_i = \mathbf{q}\cdot\mathbf{a}_i$ and $z_j = (\hat{x} + i\hat{y})\cdot\mathbf{a}_j/\sqrt{\Omega}$:

$$\mathcal{H}^{\mathbf{q}}_{mn} = \langle m | \exp\left(i\epsilon_{ij}q_iZ_j\right)|n\rangle , \ Z_j = \frac{\bar{z}_j a + z_j a^\dagger}{\sqrt{2\phi}} . \tag{27}$$

Here $i, j \in \{1, 2\}$ are the crystalline indices which are summed over. A closed-form expression for the unitary matrix $\mathcal{H}^{\mathbf{q}}$ in terms of Laguerre polynomials is provided in Eq. 140 of Ref.[38]. With Eq. (26), the action of any periodic potential on the magnetic translation group eigenbasis is easily obtained. The kinetic term in Eq. (23) does not depend on $\mathbf{k}$ because it only contains $a, a^\dagger$ operators and creates flat Landau levels. We observe that all the $\mathbf{k}$-dependence of Eq. (23) is contained in the potential term matrix elements Eq. (26) in the form $\exp(i\Omega\mathbf{k}\times\mathbf{G}) = \exp(-i(G_1k_2 - G_2k_1))$ and hence $H^{\phi=2\pi}(\mathbf{k})$ is analytic in $\mathbf{k}$. From the $\mathbf{k}$-dependence of Eq. (20), we deduce that $|\mathbf{k} + 2\pi\mathbf{G}, n\rangle = |\mathbf{k}, n\rangle$. Thus $H^{\phi=2\pi}_{mn}(\mathbf{k} + 2\pi\mathbf{G}) = H^{\phi=2\pi}_{mn}(\mathbf{k})$ is explicitly periodic in $\mathbf{k}$, so no embedding matrices[41] are required.

V. BERRY CONNECTION

Our basis of magnetic translation eigenstates (Eq. (15)) is built from continuum Landau levels. These states are known to carry a Chern number[49], and it will be important to see how this arises in our formalism. To study the topology, we need to compute the continuum Berry connection:

$$(2\pi)^2\delta(\mathbf{k}-\mathbf{k}')\mathcal{A}^{mn}(\mathbf{k}) = \langle \mathbf{k}', m|\mathbf{r}|\mathbf{k}, n\rangle \ . \tag{28}$$

In zero flux where the basis states are plane waves or Fourier transforms of localized orbitals, $\mathcal{A}^{mn}(\mathbf{k})$ would be trivial. However, the basis states at 2π flux are built out of Landau levels, which by themselves are topologically nontrivial. We can see this directly by computing $\langle \mathbf{k}', n|\mathbf{r}|\mathbf{k}, n\rangle$ (here the Landau level index n is unsummed), the Abelian Berry connection of the nth Landau level, using the oscillator algebra. The result from Ref.[38] is

$$\mathcal{A}^{nn}_i(\mathbf{k}) = -\frac{1}{2}\epsilon_{ij}\partial_j \log\vartheta\left(\frac{(k_1, k_2)}{2\pi}\middle|\,\Phi\right) \tag{29}$$

where $\partial_i = \frac{\partial}{\partial k_i}$ here for brevity, $\mathcal{A}_i = \mathbf{b}_i\cdot\mathcal{A}$, and we emphasize that $\mathcal{A}_{nn}(\mathbf{k})$ is independent of n. Interestingly, a similar formula has appeared recently in flat band Chern states in Ref.[50]. We now show that the connection Eq. (29) has Chern number -1.[51] In Ref.[38], we show with a direct computation that the Berry curvature is given by

$$\epsilon_{ij}\partial_i\mathcal{A}^{nn}_j = \frac{1}{2}\partial^2\log\vartheta = -\frac{1}{2\pi} + 2\pi\delta(\mathbf{k} - \pi\mathbf{b}_1 - \pi\mathbf{b}_2) \tag{30}$$

and has two contributions. The $-1/2\pi$ term in Eq. (30) is the constant and nonzero Berry curvature of a Landau level[29,50]. The delta function appearing at $\mathbf{k}^* = \pi\mathbf{b}_1 + \pi\mathbf{b}_2$ is an artifact of the undefined basis states at $\mathbf{k}^*$ where $\mathcal{N}(\mathbf{k}^*) = 0$ and is discussed fully in Ref.[38]. In fact, the 2π delta function is unobservable in the Wilson loop winding because the Berry phase is only defined mod 2π. To see this, we explicitly calculate the Abelian Wilson loop (or Berry phase) in Ref.[38] and show the result in Fig. 1(b) where we see that the Wilson loop eigenvalues are indeed continuous mod 2π. Hence we can think of the the basis states in Eq. (15) as lattice-regularized Landau levels. We also see that the zero in the normalization factor $\mathcal{N}(\mathbf{k})$ (see Sec. III) is an *essential* feature of the basis rather than a pathological one: it is a manifestation of the topology of the basis states. If there were no zero, then we would have written down wavefunctions which

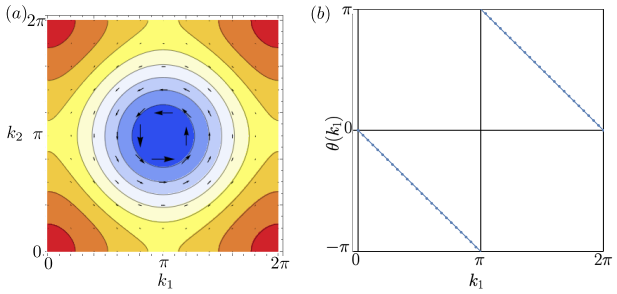

FIG. 1. (a) The Siegel theta function $\mathcal{N}(\mathbf{k})$ (see Eq. (18)) is plotted with arrows denoting the vector field $\mathcal{A}_{nn}(\mathbf{k})$. The winding in $\mathcal{A}$ around the zero located at $k_1 = \pi, k_2 = \pi$ leads to a Chern number in the *basis* states. (b) The Wilson loop $W(k_1) = e^{i\theta(k_1)}$ of a single Landau level integrated along k_2 is plotted as a function of k_1. The Wilson loop is computed analytically in Ref.[38] to be $W(k_1) = e^{-ik_1}$ (shown in solid blue) which winds once crossing the vortex at (π, π). The numerical approximation of $W(k_1)$ is dotted.

were periodic and differentiable on the entire BZ, hence precluding a Chern number[52].

Finally, we obtain an explicit expression for the non-Abelian Berry connection $\mathcal{A}^{MN}(\mathbf{k})$ in the occupied bands indexed by M, N:

$$(2\pi)^2\delta(\mathbf{k}-\mathbf{k}')\mathcal{A}^{MN}(\mathbf{k}) = \sum_{mn}[U^\dagger(\mathbf{k}')]^M_m \langle \mathbf{k}', m|\mathbf{r}|\mathbf{k}, n\rangle\, U^N_n(\mathbf{k}) \tag{31}$$

where $U(\mathbf{k})$ is the $N_{LL} \times N_{occ}$ matrix of eigenvectors. N_{occ} is the number of occupied bands and N_{LL} is the dimension of the matrix Hamiltonian, which is truncated at N_{LL} Landau levels. Leaving the details of the calculation to Ref.[38], we give the general formula

$$\begin{aligned}\mathcal{A}_i^{MN}(\mathbf{k}) &= [U^\dagger(i\partial_i - \epsilon_{ij}\tilde{Z}_j)U]^{MN} \\ &\quad - \frac{\delta^{MN}}{2}\epsilon_{ij}\partial_j \log\vartheta\left(\frac{(k_1,k_2)}{2\pi}\middle|\,\Phi\right).\end{aligned} \tag{32}$$

The Abelian term in the second line of Eq. (32) describes the Chern numbers of the basis states as in Eq. (29). Note that it is proportional to the identity δ^{MN} and so can be factored out of the Wilson loop to give an overall winding factor per Landau level as shown in Fig. 1(b). The new non-Abelian term $U^\dagger\tilde{Z}_jU$ of Eq. (32) describes coupling between Landau levels where the Hermitian matrix $[\tilde{Z}_j]_{mn} = \langle m|Z_j|n\rangle$ is given in Eq. (27). Returning to Eq. (32), we write the non-Abelian Wilson loop as the path-ordered matrix exponential

$$\begin{aligned}[W_\mathcal{C}]^{MN} &= \left[\exp\left(i\oint_\mathcal{C} d\mathbf{k}\cdot\mathcal{A}(\mathbf{k})\right)\right]^{MN} \\ &= e^{-i\oint_\mathcal{C} d\mathbf{k}\times\frac{1}{2}\boldsymbol{\nabla}\log\vartheta\left(\frac{(k_1,k_2)}{2\pi}\middle|\Phi\right)} \\ &\quad\times\left[\exp\left(i\oint_\mathcal{C} dk_i\, U^\dagger(i\partial_i - \epsilon_{ij}\tilde{Z}_j)U\right)\right]^{MN}\end{aligned} \tag{33}$$

with a sum over i, j implied. For numerical computations, Eq. (33) should be expanded into an ordered product form using the projectors $P_\mathbf{k} = U(\mathbf{k})U^\dagger(\mathbf{k})$. This procedure can be carried through exactly (the details may be found in Ref.[38]) and the result is

$$\begin{aligned}W_\mathcal{C} &= \exp\left[-i\oint_\mathcal{C} d\mathbf{k}\times\frac{1}{2}\boldsymbol{\nabla}\log\vartheta\left(\frac{(k_1,k_2)}{2\pi}\middle|\,\Phi\right)\right] \\ &\quad\times U^\dagger(\mathbf{k}_L)\mathcal{H}^{-d\mathbf{k}_L}\left(\prod_n^{(L-1)\leftarrow 1} P(\mathbf{k}_n)\mathcal{H}^{-d\mathbf{k}_n}\right)U(\mathbf{k}_0)\end{aligned} \tag{34}$$

where $\mathcal{C}$ is a closed path with starting at $\mathbf{k}_1$ which is broken into L segments labeled by $\mathbf{k}_n$, and $d\mathbf{k}_n = \mathbf{k}_n - \mathbf{k}_{n-1}$. The insertions of non-Abelian terms $\mathcal{H}^{d\mathbf{k}} = e^{i\epsilon_{ij}dk_i\tilde{Z}_j}$ act off-diagonally on the Landau level index (see Eq. (27)). The appearance of these non-Abelian terms reflects the fact that the Landau level states in Eq. (15) are not localized below the magnetic length, which is $1/\sqrt{\phi}$ in dimensionless units. In Sec. VI, we use the results of this section to calculate the Wilson loop in a square lattice model tuned through a topological phase transition at 2π flux by increasing the strength of the crystalline potential.

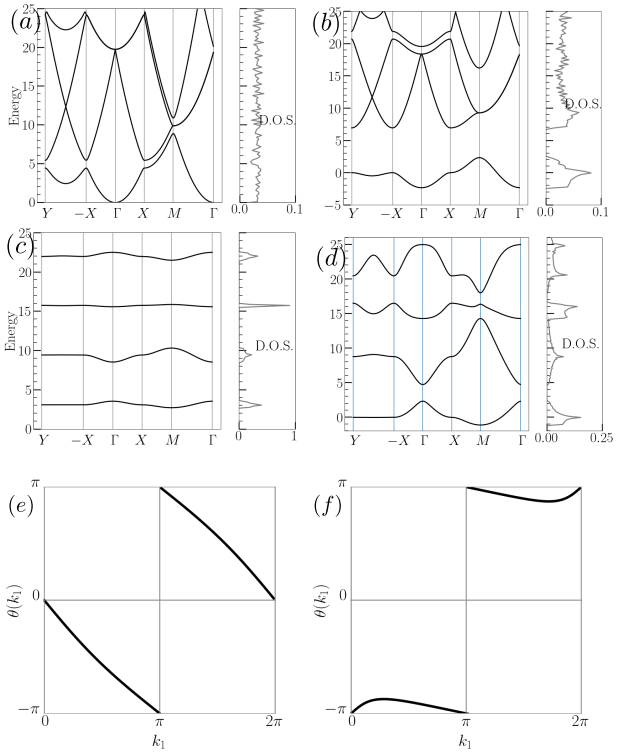

FIG. 2. (a, b) Square lattice in zero flux, at low potential $w = 1$ and high potential $w = 7$ respectively. (c, d) Square lattice in 2π flux, at low potential and high potential respectively. (e, f) Wilson loops of the square lattice in flux. At low hoppings, the Hamiltonian resembles a Landau level system, resulting in nearly flat bands and a winding in the Wilson loop for the lowest band. At large hoppings, a gap closing occurs and allows the lowest band to have Chern number zero.

VI. SQUARE LATTICE EXAMPLE

The simplicity of implementing our formalism is illustrated with a model of a scalar particle mass $m = 1$ which feels a square lattice cosine potential. While it may be possible to simulate this type of model on an optical lattice[53–55], we intend this example to be pedagogical rather than physically motivated. We take the lattice vectors and reciprocal vectors to be $\mathbf{a}_1 = \mathbf{b}_1 = (1, 0), \mathbf{a}_2 = \mathbf{b}_2 = (0, 1)$ so $\Omega = 1$ and define the zero-flux Hamiltonian as

$$H^{\phi=0} = -\frac{1}{2}\boldsymbol{\nabla}^2 + \frac{w}{2}(e^{-2\pi i\mathbf{b}_1\cdot\mathbf{r}} + e^{-2\pi i\mathbf{b}_2\cdot\mathbf{r}} + H.c.), \tag{35}$$

where we have taken $\hbar = 1$. When $w = 0$, the Hamiltonian $H^{\phi=0}$ has continuous translation symmetry and solutions can be labeled by momentum $\mathbf{k}$. When w is nonzero, the continuous translation symmetry is broken

to a discrete symmetry which weakly couples the plane wave states and opens gaps at the corners of the BZ. By Bloch's theorem, the states are labeled by momentum $\mathbf{k}$ in the BZ and the effective Hamiltonian reads

$$H^{\phi=0}_{\mathbf{G},\mathbf{G}'}(\mathbf{k}) = \frac{1}{2}(\mathbf{k}-\mathbf{G})^2\delta_{\mathbf{G}\mathbf{G}'} + \frac{w}{2}(\delta_{\mathbf{G},\mathbf{G}'-2\pi\mathbf{b}_1} + \delta_{\mathbf{G},\mathbf{G}'-2\pi\mathbf{b}_2} + H.c.) \tag{36}$$

and $\mathbf{G} = G_1\mathbf{b}_1 + G_2\mathbf{b}_2, G_i \in \mathbb{Z}$ (see Ref.[38] for details). We show the Bloch band structure in Fig. 2 in the weak and strong potential regimes. In flux, the Hamiltonian Eq. (35) is written in terms of the canonical momentum

$$H^{\phi} = \frac{1}{2}\boldsymbol{\pi}^2 + \frac{w}{2}(e^{-2\pi i\mathbf{b}_1\cdot\mathbf{r}} + e^{-2\pi i\mathbf{b}_2\cdot\mathbf{r}} + H.c.), \tag{37}$$

that is, Landau levels in a lattice potential. In 2π flux using the matrix elements in Eq. 139 of Ref.[38], the magnetic Bloch Hamiltonian is

$$H^{\phi=2\pi}_{mn}(\mathbf{k}) = \phi(m+\frac{1}{2})\delta_{mn} + \frac{w}{2}(e^{-ik_2}\mathcal{H}^{2\pi\mathbf{b}_1}_{mn} + e^{ik_1}\mathcal{H}^{2\pi\mathbf{b}_2}_{mn} + H.c.) \tag{38}$$

and recalling that the kinetic term acts on the $|\mathbf{k}, m\rangle$ basis as $\frac{1}{2}\boldsymbol{\pi}^2 = \phi(a^\dagger a + \frac{1}{2})$. The potential term $\mathcal{H}^{2\pi\mathbf{G}}_{mn}$ couples the Landau levels, giving nontrivial dispersion. We numerically calculate the band structure in the weak coupling ($w = 1$) and strong coupling ($w = 7$) regimes. The Landau level regime in weak coupling exhibits nearly flat bands (Fig. 2(c)), and its lowest band carries a Chern number, as exemplified by the winding of the Wilson loop shown in Fig. 2(e). Increasing w pushes the model through a phase transition with a band touching at the Γ point. At strong coupling ($w = 7$), the 2π flux spectrum is gapped (Fig. 2(d)) and its lowest band has zero Chern number (Fig. 2(f)). Hence the lowest band cannot be interpreted as a Landau level, despite the strong flux.

VII. MANY-BODY FORM FACTORS

Thus far, we have discussed the single-particle spectrum and Wilson loop topology of continuum Hamiltonians at 2π flux. In this section, we extend our formalism to many-body physics and derive a convenient expression for the Coulomb Hamiltonian

$$H_{int} = \frac{1}{2}\int d^2r d^2r'\, n(\mathbf{r})V(\mathbf{r}-\mathbf{r}')n(\mathbf{r}') \tag{39}$$

in terms of the magnetic translation operator eigenbasis Eq. (15). Here $n(\mathbf{r}) = c^\dagger(\mathbf{r})c(\mathbf{r})$ is the local density operator at $\mathbf{r}$ and $c(\mathbf{r}), c^\dagger(\mathbf{r})$ are the continuum fermion operators satisfying $\{c^\dagger(\mathbf{r}), c(\mathbf{r}')\} = \delta(\mathbf{r}-\mathbf{r}')$. In Sec. IX, we will project the Coulomb interaction on the flat bands of TBG in order to study its many-body insulating groundstates, as done in zero flux in Refs.[56,57]. The calculation for TBG is more involved because there are additional indices corresponding to valley and spin (see Ref.[38] for details). For simplicity, we focus on models with only a single orbital per unit cell in this section and study the projected Coulomb Hamiltonian at 2π flux.

To avoid confusion with the Fock space braket notation in many-body calculations, we return to a wavefunction notation for the magnetic translation group eigenstates:

$$\psi_{\mathbf{k},n}(\mathbf{r}) = \frac{1}{\sqrt{\mathcal{N}(\mathbf{k})}}\sum_{\mathbf{R}} e^{-i\mathbf{k}\cdot\mathbf{R}}T^{\mathbf{b}_1\cdot\mathbf{R}}_{\mathbf{a}_1}T^{\mathbf{b}_2\cdot\mathbf{R}}_{\mathbf{a}_2}\frac{a^{\dagger n}}{\sqrt{n!}}\psi_0(\mathbf{r}), \tag{40}$$

where ψ_0 is the zeroth Landau level $a\psi_0 = b\psi_0 = 0$. Throughout this section, $|0\rangle$ is the Fock vacuum satisfying $c(\mathbf{r})|0\rangle = 0$ (not the Landau level vacuum) as is clear from context. The second-quantized creation operators $\psi^\dagger_{\mathbf{k},n}$ are defined by

$$\langle\mathbf{r}|\,\psi^\dagger_{\mathbf{k},n}|0\rangle = \langle 0|c_{\mathbf{r}}\psi^\dagger_{\mathbf{k},n}|0\rangle = \psi_{\mathbf{k},n}(\mathbf{r}) \tag{41}$$

and $\{\psi^\dagger_{\mathbf{k}',m}, \psi_{\mathbf{k},n}\} = (2\pi)^2\delta_{mn}\delta(\mathbf{k}-\mathbf{k}')$. We study the a general density-density interaction (essentially the Coulomb interaction with arbitrary screening) which can be put into the form

$$H_{int} = \frac{1}{2}\int d^2r d^2r'\, n(\mathbf{r})V(\mathbf{r}-\mathbf{r}')n(\mathbf{r}') = \frac{1}{2}\int \frac{d^2q}{(2\pi)^2}\,V(\mathbf{q})\rho_{-\mathbf{q}}\rho_{\mathbf{q}}, \quad \rho_{\mathbf{q}} = \int d^2r\, e^{-i\mathbf{q}\cdot\mathbf{r}}n(\mathbf{r}) \tag{42}$$

where $V(\mathbf{q})$ is the Fourier transform of the position-space potential. Throughout, we use $\mathbf{q} = \mathbf{k} + 2\pi\mathbf{G}$ to denote a continuum momentum. We assume that $V(\mathbf{q}) > 0$ but is otherwise fully general. Our goal is to express the Fourier modes $\rho_{\mathbf{q}}$ in terms of the $\psi^\dagger_{\mathbf{k},m}$ operators. This is accomplished by calculating the matrix elements $\langle 0|\psi_{\mathbf{k},m}\rho_{\mathbf{q}}\psi^\dagger_{\mathbf{k}',n}|0\rangle$ because $\rho_{\mathbf{q}}$ is a one-body operator. The calculation is performed in Ref.[38], and yields

$$\rho_{\mathbf{q}} = \sum_{mn}\int \frac{d^2k}{(2\pi)^2}e^{i\xi_{\mathbf{q}}(\mathbf{k})}\psi^\dagger_{\mathbf{k}-\mathbf{q},m}\mathcal{H}^{\mathbf{q}}_{mn}\psi_{\mathbf{k},n}, \tag{43}$$

with the phase factor $\xi_{\mathbf{q}}(\mathbf{k})$ defined by

$$e^{i\xi_{\mathbf{q}}(\mathbf{k})} = \frac{e^{-\frac{\bar{q}q}{4\phi}}\vartheta\left(\frac{(k_1-q/2,k_2+iq/2)}{2\pi}\middle|\,\Phi\right)}{\sqrt{\vartheta\left(\frac{(k_1,k_2)}{2\pi}\middle|\,\Phi\right)\vartheta\left(\frac{(k_1-q_1,k_2-q_2)}{2\pi}\middle|\,\Phi\right)}}. \tag{44}$$

with $q = (\mathbf{a}_1 + i\mathbf{a}_2)\cdot\mathbf{q}$. The unitary matrix $\mathcal{H}^{\mathbf{q}}$ defined in Eq. (27). We prove analytically that $e^{i\xi_{\mathbf{q}}(\mathbf{k})}$ is a pure phase at the end of Ref.[38]. At $\mathbf{k} = \pi\mathbf{b}_1 + \pi\mathbf{b}_2$ and $\mathbf{k} = \pi\mathbf{b}_1 + \pi\mathbf{b}_2 + \mathbf{q}$, the denominator of Eq. (44) has zeroes which are exactly canceled by the zeros of the numerator (they are removable singularities), so $\xi_{\mathbf{q}}(\mathbf{k})$ is always real. We plot $\xi_{\mathbf{q}}(\mathbf{k})$ in Fig. 3 which shows that a branch cut

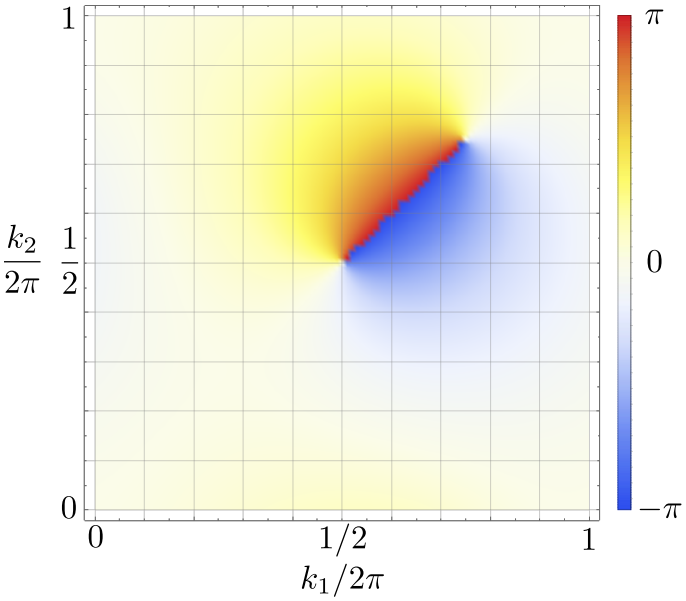

FIG. 3. Phase $\xi_{\mathbf{q}}(\mathbf{k})$ in Eq. 44 for $\mathbf{q} = \frac{\pi}{2}\mathbf{b}_1 + \frac{\pi}{2}\mathbf{b}_2$, plotted as a density. Note the branch cut linking $(1/2, 1/2)$ to $(3/4, 3/4)$.

connects the removable singularities at (π, π) and $(\pi + q_1, \pi + q_2)$.

So far, we have developed an expression for the density operators (Eq. (43)) and thus for the many-body Coulomb Hamiltonian in terms of the single-particle magnetic translation group eigenstates. This will make it possible to perform a projection onto a set of low-energy bands. To do so, define the energy eigenstate operator $\gamma^\dagger_{\mathbf{k},N}$ that creates state at momentum $\mathbf{k}$ in band N:

$$\gamma^\dagger_{\mathbf{k},N} = \sum_m U^N_m(\mathbf{k})\psi^\dagger_{\mathbf{k},m}, \tag{45}$$

with $U^N(\mathbf{k})$ the eigenvector of the Hamiltonian corresponding to band N. (In models with more orbitals indexed by α, Eq. (45) would also contain a sum over α.) In second quantized notation, we arrive at the general expression

$$\rho_{\mathbf{q}} = \int \frac{d^2k}{(2\pi)^2} \sum_{MN} \gamma^\dagger_{\mathbf{k}-\mathbf{q},M} M_{MN}(\mathbf{k},\mathbf{q})\gamma_{\mathbf{k},N}, \tag{46}$$

where the form factor matrix $M(\mathbf{k},\mathbf{q})$ obtained from Eq. (46) is defined as

$$M_{MN}(\mathbf{k},\mathbf{q}) = e^{i\xi_{\mathbf{q}}(\mathbf{k})}[U^\dagger(\mathbf{k}-\mathbf{q})\mathcal{H}^{\mathbf{q}}U(\mathbf{k})]_{MN}\ . \tag{47}$$

Note that $M(\mathbf{k},\mathbf{q})$ is not a gauge-invariant quantity because the eigenvectors in the matrices $U(\mathbf{k})$ and $U(\mathbf{k}-\mathbf{q})$ are only defined up to overall phases (or in general unitary transformations if there are degeneracies in the bands). Ref.[38] contains a complete discussion, which we summarize by noting the "gauge freedom" taking $M(\mathbf{k},\mathbf{q}) \to W^\dagger(\mathbf{k}-\mathbf{q})M(\mathbf{k},\mathbf{q})V(\mathbf{k})$ where $W(\mathbf{k}-\mathbf{q}), V(\mathbf{k})$ are arbitrary unitary matrices. There are gauge-invariant quantities determined from $M(\mathbf{k},\mathbf{q})$ such as its singular values, which are the eigenvalues of $M^\dagger(\mathbf{k},\mathbf{q})M(\mathbf{k},\mathbf{q})$. We will use the singular values to study the flat metric condition[58] in Sec. IX A.

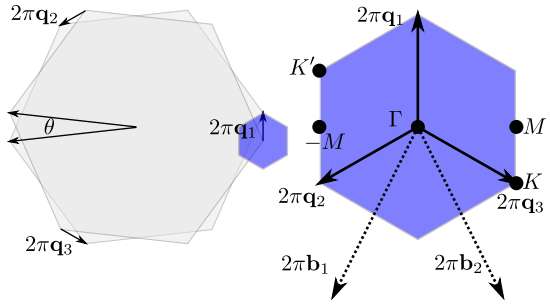

FIG. 4. Construction and conventions of the moiré BZ, blue hexagon, from the graphene layers with relative twist θ.

Having discussed the form factors, we emphasize that Eq. (46) is an exact expression for the density operator. To define a projected density operator, we restrict the indices M, N to a subset of low-energy bands so that $\rho_{\mathbf{q}}$ annihilates all other bands. Our result in Eq. 46 is structurally similar to the form factor expression obtained in Ref.[58] in zero flux. We discuss the behavior of the form factor in Ref.[38].

VIII. TWISTED BILAYER GRAPHENE: SINGLE-PARTICLE PHYSICS

Twisted bilayer graphene (TBG) is a metamaterial formed from twisting two graphene sheets by a relative angle θ[14,59,60]. The resulting moiré pattern is responsible for the very large unit cell that allows experimental access to $\phi = 2\pi$. Let us set our conventions for the geometry of the moiré twist unit cell. First, the graphene unit cell has a lattice vector of length $a_g = .246$nm and an area $\Omega_g = a_g^2\frac{\sqrt{3}}{2}$. The monolayer graphene K point is $\mathbf{K}_g = \frac{2\pi}{a_g}(0, 2/3)$. The moiré vectors $\mathbf{q}_j$ are defined by the difference in momentum space of the rotated layers' K points:

$$\begin{aligned} &2\pi\mathbf{q}_1 = (R_{\theta/2} - R_{-\theta/2})\mathbf{K}_g, \quad \mathbf{q}_j = C_3\mathbf{q}_{j-1}, \\ &2\pi|\mathbf{q}_j| \equiv k_\theta = 2|\mathbf{K}_g|\sin\frac{\theta}{2} = \frac{8\pi\sin\frac{\theta}{2}}{3a_g} \end{aligned} \tag{48}$$

where R_θ is a 2D rotation matrix. The moiré reciprocal lattice vectors are defined

$$\mathbf{b}_j = \mathbf{q}_j - \mathbf{q}_3, \quad \mathbf{b}_1 \times \mathbf{b}_2 = \frac{(2\sin\frac{\theta}{2})^2}{\Omega_g}\ . \tag{49}$$

The moiré lattice is defined by $\mathbf{a}_i \cdot \mathbf{b}_j = \delta_{ij}$ which yields

$$\mathbf{a}_1 = \frac{a_g}{2\sin\frac{\theta}{2}}\{-\frac{\sqrt{3}}{2}, -\frac{1}{2}\} \quad \mathbf{a}_2 = \frac{a_g}{2\sin\frac{\theta}{2}}\{\frac{\sqrt{3}}{2}, -\frac{1}{2}\}\ . \tag{50}$$

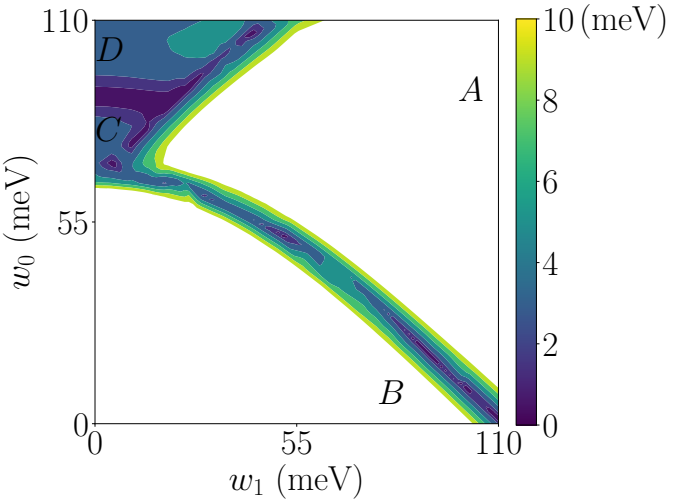

FIG. 5. Phase diagram of TBG in 2π flux at magic angle. We plot the gap between the flat and passive bands as a function of parameters w_0, w_1. Phase A, containing the physical TBG parameters is in the crystalline regime where the flat bands have zero Chern number, while phase B is connected to the Landau level limit where each flat band has Chern number -1. The first chiral limit where w_0 is in phase B at $w_1 = 110$meV. C and D are phases connected to the second chiral limit $w_1 = 0$ where the bands have strong dispersion (see Fig. 6).

Finally, the moiré unit cell has area

$$\Omega = \mathbf{a}_1 \times \mathbf{a}_2 = \frac{\Omega_g}{(2\sin\frac{\theta}{2})^2} \ . \tag{51}$$

The moiré Brillouin zone is depicted in Fig. 4. At the magic angle where $\theta = 1.05°$, the moiré unit cell is ~ 3000 times larger than the graphene unit cell. The magnetic translation group commutes when $\phi = \frac{eB\Omega}{\hbar} = 2\pi$, which occurs at $B \in (25, 32)$T for $\theta \in (1.03°, 1.15°)$. These fields are experimentally accessible, making it possible to explore the Hofstadter regime of TBG. Ref.[33] focuses on TBG at the magic angle, as well as the evolution of the spectrum in flux.

The following sections contain a thorough treatment of TBG at 2π flux. We discuss the Bistritzer-MacDonald (BM) Hamiltonian in Sec. VIII A and show the phase diagram of TBG, identifying a crystalline regime (including the physical TBG parameters) where the flat bands have vanishing Chern number and a Landau level regime (including the first chiral limit) where the flat bands each have Chern number -1, denoted by A and B respectively in the phase diagram Fig. 5. In Sec. VIII A, we discuss the symmetries, topology, and Wannier functions which are different than at zero flux. Importantly, we find that the $C_{2z}\mathcal{T}$ symmetry, which is essential in protecting the nontrivial topology at $\phi = 0$, is broken. At $\phi = 2\pi$, we find that the TBG flat band structure can be obtained from atomic limits but still has Wannier functions pinned to the corners of the moiré unit cells. In Sec. VIII C, we focus on the chiral limit of TBG where the chiral anomaly, a well-studied feature of relativistic gauge theory[61–69], protects a pair of perfectly flat bands in TBG at all angles at 2π flux.

A. Band structure

We begin with the Bistritzer-MacDonald model of twisted bilayer graphene in the untwisted graphene K valley (and arbitrary spin) at zero flux:

$$H_{BM} = \begin{pmatrix} -i\hbar v_F \boldsymbol{\sigma}\cdot\boldsymbol{\nabla} & T^\dagger(\mathbf{r}) \\ T(\mathbf{r}) & -i\hbar v_F \boldsymbol{\sigma}\cdot\boldsymbol{\nabla} \end{pmatrix}, \tag{52}$$

with σ labeling the sublattice degree of freedom and the 2×2 matrix notation labeling the layer index. Note that H_{BM} neglects the twist angle dependence in the kinetic term and thus has an exact particle-hole symmetry[60]. For simplicity, we work in this approximation, but we note that incorporating the twist angle dependence poses no essential difficulty for our formalism. The moiré potential is $T(\mathbf{r}) = \sum_{j=1}^{3} e^{2\pi i \mathbf{q}_j\cdot\mathbf{r}} T_j$ where

$$T_{j+1} = w_0\sigma_0 + w_1\left(\sigma_1\cos\frac{2\pi}{3}j + \sigma_2\sin\frac{2\pi}{3}j\right). \tag{53}$$

To add flux into H_{BM}, we employ the canonical substitution $-i\hbar\boldsymbol{\nabla} \to \boldsymbol{\pi}$. As written, H_{BM} is not translation-invariant: the $\mathbf{q}_i$ vectors which appear in the moiré potential are not reciprocal lattice vectors. However, H_{BM} can be made translation invariant by a unitary transformation:

$$V_1 = \begin{pmatrix} e^{i\pi\mathbf{q}_1\cdot\mathbf{r}} & 0 \\ 0 & e^{-i\pi\mathbf{q}_1\cdot\mathbf{r}} \end{pmatrix} \tag{54}$$

which acts only on the layer index.[70] Acting on the states, V_1 shifts the momentum in the different layers by $2\pi\mathbf{q}_1$, reflecting separation of the Dirac points in Fig. 4. We then define the Hamiltonian in flux by

$$\begin{aligned} H^\phi_{BM}(\mathbf{r}) &= V_1 \begin{pmatrix} v_F\boldsymbol{\sigma}\cdot\boldsymbol{\pi} & T^\dagger(\mathbf{r}) \\ T(\mathbf{r}) & v_F\boldsymbol{\sigma}\cdot\boldsymbol{\pi} \end{pmatrix} V_1^\dagger \\ &= \begin{pmatrix} v_F\boldsymbol{\sigma}\cdot\boldsymbol{\pi} - \pi v_F\mathbf{q}_1\cdot\boldsymbol{\sigma} & \tilde{T}^\dagger(\mathbf{r}) \\ \tilde{T}(\mathbf{r}) & v_F\boldsymbol{\sigma}\cdot\boldsymbol{\pi} + \pi v_F\mathbf{q}_1\cdot\boldsymbol{\sigma} \end{pmatrix} \end{aligned} \tag{55}$$

with $\tilde{T}(\mathbf{r}) = T_1 + T_2 e^{2\pi i\mathbf{b}_1\cdot\mathbf{r}} + T_3 e^{2\pi i\mathbf{b}_2\cdot\mathbf{r}}$. In this form, the matrix elements of $\tilde{T}(\mathbf{r})$ in the magnetic translation operator basis can be directly obtained with Eq. 139 in Ref.[38] in a sublattice/Landau level tensor product basis. An explicit expression is given in Eq. 228 of Ref.[38]. The kinetic term can be expressed simply with Landau level operators. Expanding the Pauli matrices, we find

$$\begin{aligned} v_F\boldsymbol{\sigma}\cdot\boldsymbol{\pi} &= v_F\sqrt{2eB}\begin{pmatrix} 0 & a^\dagger \\ a & 0 \end{pmatrix} = v_F\sqrt{2\phi/\Omega}\begin{pmatrix} 0 & a^\dagger \\ a & 0 \end{pmatrix} \\ &= v_F k_\theta \left(\frac{3\sqrt{3}}{2\pi}\right)^{1/2}\begin{pmatrix} 0 & a^\dagger \\ a & 0 \end{pmatrix} \end{aligned} \tag{56}$$

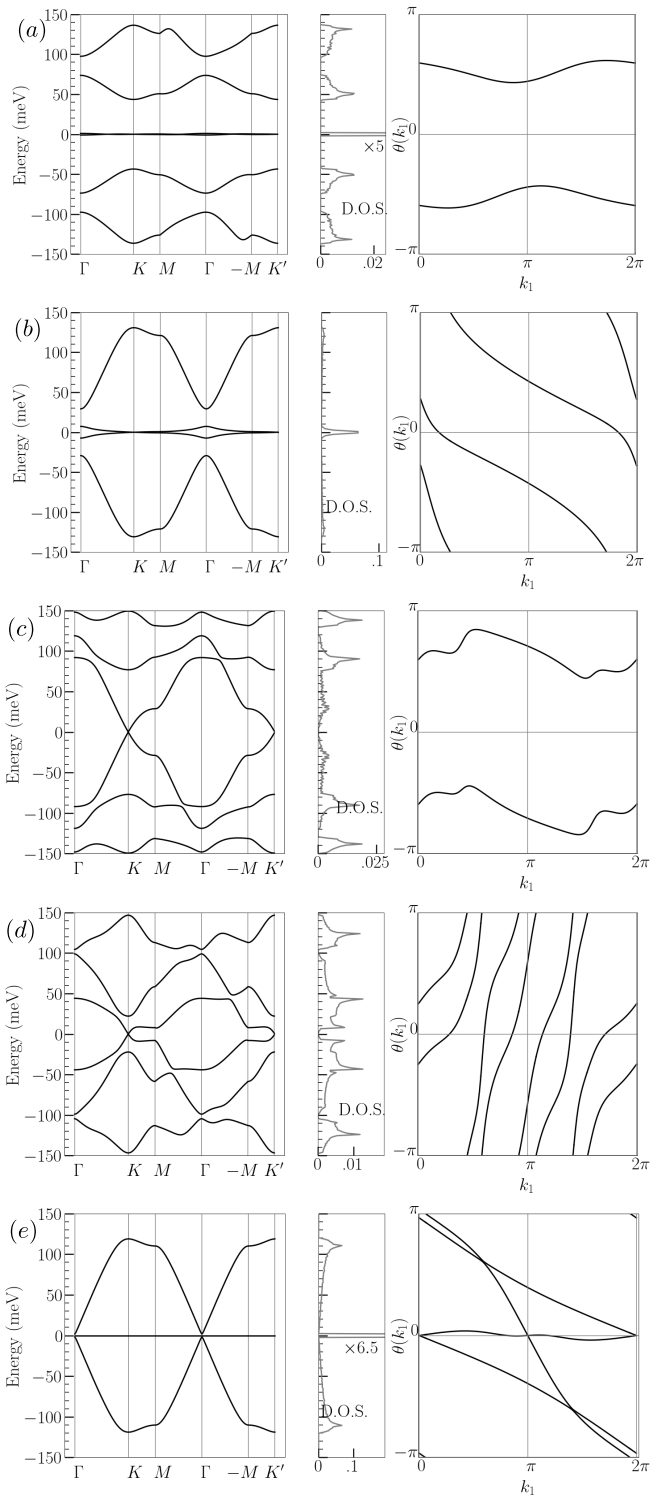

FIG. 6. Band structures (left), density of states (middle), and Wilson loops (right) of TBG at 2π flux. The parameters $\left(\sqrt{3}w_0/(v_F k_\theta), \sqrt{3}w_1/(v_F k_\theta)\right)$ given by (a): $(0.8, 1)$, (b): $(0.05, 0.8)$, (c): $(0.7, 0.15)$, (d): $(0.97, 0.32)$, (e): $(0.0, 1.0)$. (a-d) are chosen to be connected to phases $A - D$ (see Fig. 5), and (e), the chiral limit, is connected to B but has a very small gap (< 2meV). The very small gap makes the flat band Wilson loop ill-conditioned, so we compute the Wilson loop of the middle 4 bands.

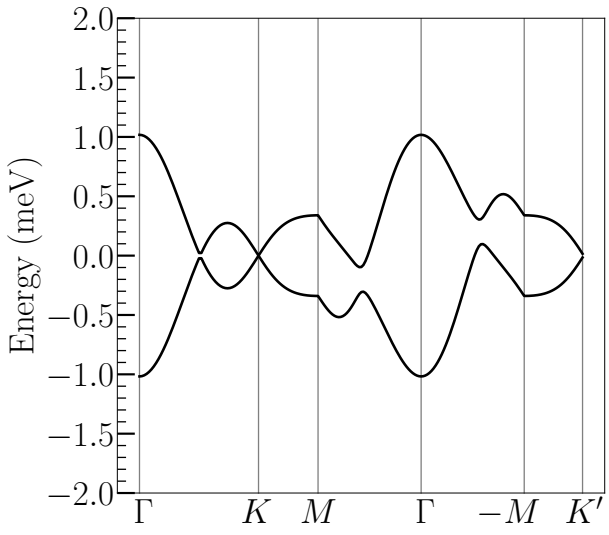

FIG. 7. Close-up of the flat bands of TBG in flux at magic angle. Note the protected Dirac points at K, K' due to the different C_3 eigenvalues of the flat bands (see Eq. (59)) and MT, P symmetries, as well as the maximal gap at Γ where the C_3 eigenvalues are the same.

using $\phi = 2\pi$ and the moiré wavevector k_θ in Eq. (48). The numerical factor coming from the unit cell geometry is $(3\sqrt{3}/2\pi)^{1/2} \simeq .91$. Lastly, the momentum shift $\pi v_F \mathbf{q}_1 \cdot \boldsymbol{\sigma}$ in Eq. (55) acts as the identity on the Landau level index, and $\pi v_F \mathbf{q}_1 \cdot \boldsymbol{\sigma} = \frac{v_F k_\theta}{2}\sigma_2$ using $2\pi \mathbf{q}_1 = k_\theta \hat{y}$. The Dirac Hamiltonian Eq. (56) in flux is well-studied. At 2π flux and $\theta = 1.05°$, the low energy spectrum of Eq. (56) consists of a zero mode and states at $\pm E_1 = \pm .91 v_F k_\theta = \pm 170$meV. This is on the same scale as the potential strength $w_1 = 110$meV.

Numerical analysis of the band structure is straightforward and yields two flat bands (per valley and spin, or 8 total) gapped from the dispersive bands by approximately 40 meV. See Fig. 6(a) for the band structure, density-of-states, and the Wilson loop of the flat bands for TBG, Fig. 6(b-e) for other choices of parameters w_0, w_1. For a close-up of the flat-band dispersion at the magic angle see Fig. 7.

B. Symmetries and Topology

In zero flux, the topology of the TBG flat bands is protected by $C_{2z}\mathcal{T}$ symmetry[60,72,73]. However, $C_{2z}\mathcal{T}$ is broken in nonzero flux because $\mathcal{T}$ reverses the magnetic field and C_{2z} preserves it[41]. On the lattice in the Peierls approximation, $C_{2z}\mathcal{T}$ is restored as a (projective) symmetry at certain values of the flux[41], but we do not consider this approximation here. In this section, we show that the band representation of TBG at $\phi = 2\pi$ can be obtained from inducing atomic orbitals at the corners of the moiré unit cell, so the fragile topology at $\phi = 0$ is broken by magnetic field. However, we find that band repre-

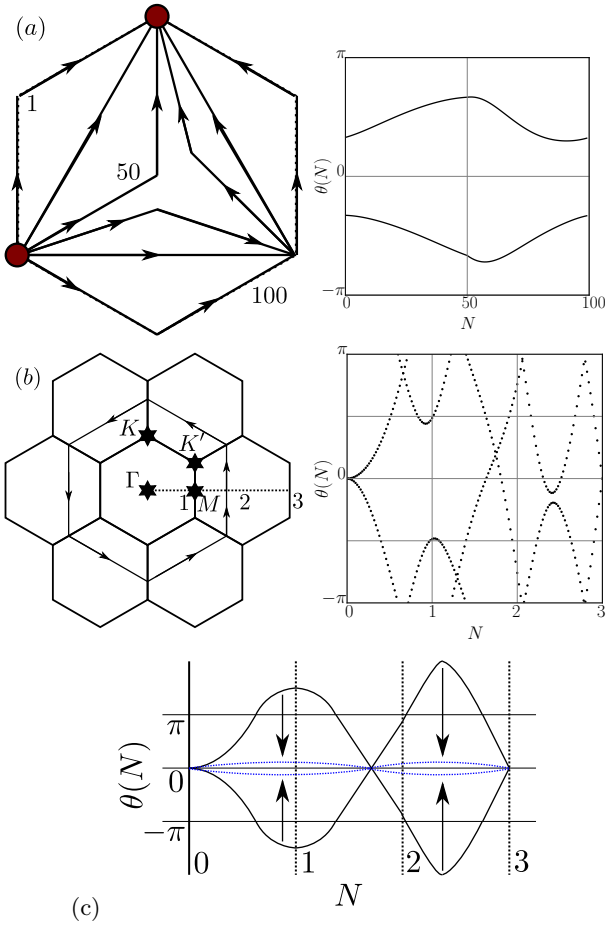

FIG. 8. C_3-symmetric Wilson loops, discussed in Refs.[60,71]. In (a), the path 1 begins at K, goes to K', then back to K. The midpoint of the path is continuously changed until Γ at 50; further paths then follow a more complicated trajectory linking K back to K and then back again. In (b), Wilson loops are taken in successively larger hexagons surrounding the Γ point. Neither loop has nontrivial winding because there are no symmetries that protect crossings at $\pm\pi$, so the Wilson loops can be deformed to flat lines as depicted in (c) which shows a caricature of the deformation process.

sentation is decomposable[39,71,74,75], so the flat bands are topologically nontrivial when gapped from each other via a particle-hole breaking term.

First we review the topology in zero flux which is discussed comprehensively in Refs.[60,72]. The space group of TBG is $p6'2'2$ which is generated by $C_3, C_{2z}\mathcal{T}$, and C_{2x}.[76] The symmetries are: three-fold rotations around the AA moiré site C_3, spacetime inversion $C_{2z}\mathcal{T}$, and two-fold rotation around the x-axis C_{2x}. Note that in 2D, C_{2x} is indistinguishable from M_y, a mirror taking $y \to -y$. The band representation of the flat bands is

$$\mathcal{B}^{\phi=0} = \Gamma_1 + \Gamma_2 + K_2K_3 + M_1 + M_2 \tag{57}$$

and the irreps are defined at the high symmetry momenta $\Gamma = (0,0), K = 2\pi\mathbf{q}_1, M = \pi\mathbf{b}_1$ by

$$\begin{array}{c|ccc} 6'm'm & 1 & C_3 & M_y \\ \hline \Gamma_1 & 1 & 1 & 1 \\ \Gamma_2 & 1 & 1 & -1 \end{array}, \quad \begin{array}{c|cc} 6' & 1 & C_3 \\ \hline K_2K_3 & 2 & -1 \end{array}, \quad \begin{array}{c|cc} 2'm'm & 1 & C_{2x} \\ \hline M_1 & 1 & 1 \\ M_2 & 1 & -1 \end{array}. \tag{58}$$

The presence of the anti-unitary $C_{2z}\mathcal{T}$ ($PC_{2z}\mathcal{T}$) symmetry in the space group is required to prove that the band representation $\mathcal{B}^{\phi=0}$ is fragile (stable) topological[60,72].

At 2π flux, the $C_{2z}\mathcal{T}$ and C_{2x} symmetries are broken because they reverse the magnetic field[41]. The resulting band topology is mentioned in Ref.[33], which we review here for completeness. Without $C_{2z}\mathcal{T}$, the topology of the flat bands is not protected. The most direct way to see this is from the Wilson loop (see Eq. (33)) integrated along $\mathbf{b}_2$ in Fig. 8(a) which shows no relative winding. The same Wilson loop at zero flux has $C_{2z}\mathcal{T}$-protected relative winding[60]. We also plot the C_3-symmetric Wilson loops discussed in Refs. 60 and 71 and find no winding, as shown in Fig. 8(a,b). The lack of winding in any Wilson loop suggests that localized, symmetry-respecting Wannier states may be formed from the two TBG flat bands at 2π flux (per valley per spin)[74,77]. Below, we discuss the flat bands in detail from the perspective of topological quantum chemistry.

At 2π flux, the 2D space group is reduced to $p31m'$ (the $k_z = 0$ plane of the 3D space group 157.55 in the BNS setting) generated by C_3 and $M\mathcal{T} \equiv C_{2x}C_{2z}\mathcal{T}$. The full algebra, including the anti-commuting unitary P symmetry, is

$$\begin{gathered} M\mathcal{T}C_3 = C_3^\dagger M\mathcal{T}, \quad C_3^3 = 1 \\ [P, C_3] = 0, \quad P^2 = -1 \\ \{P, M\mathcal{T}\} = 0 \quad (M\mathcal{T})^2 = +1 \end{gathered}$$

and their action on the Hamiltonian is

$$\begin{aligned} C_3 H^{\phi=2\pi}(\mathbf{k}) C_3^\dagger &= H^{\phi=2\pi}(C_3\mathbf{k}), \\ M\mathcal{T} H^{\phi=2\pi}(k_x, k_y)(M\mathcal{T})^{-1} &= H^{\phi=2\pi}(k_x, -k_y), \\ P H^{\phi=2\pi}(\mathbf{k}) P^\dagger &= -H^{\phi=2\pi}(-\mathbf{k}). \end{aligned} \tag{59}$$

The operator $\mathcal{P} = PM\mathcal{T}$ squares to $+1$ and satisfies $\mathcal{P}C_3 = C_3^2\mathcal{P}$. $\mathcal{P}$ sends $(k_x, k_y) \to (-k_x, k_y)$ and hence is local at the K and K' points. Because $\mathcal{P}$ anticommutes with the Hamiltonian at Γ, K, and K', it switches the two flat bands if they are at nonzero energies $\pm E$. If $\mathcal{P}|\Psi_{+E}\rangle = |\Psi_{-E}\rangle$ and $|\Psi_{+E}\rangle$ carries C_3 eigenvalue ω, then $|\Psi_{-E}\rangle$ also carries eigenvalue ω. For the Γ point this is indeed what happens – we find the Γ point is gapped in Fig. 7 – but the K, K' points cannot gap, as a Dirac cone carries different C_3 eigenvalues in the two flat bands.

Ref.[41] demonstrated that no symmetries or topology protect a gap closing between the flat bands and passive bands at nonzero flux, matched by experimental evidence in Refs.[34,78]. As such, the irreps in nonzero flux are obtained from $\mathcal{B}^{\phi=0}$ by reduction to the $p31m'$ subgroup of $p6'2'2$. We use the Bilbao Crystallographic Server[79,80] to determine the irreps and elementary band representations of $p31m'$. They may be found at `https://www.cryst.ehu.es/cgi-bin/cryst/programs/mbandrep.pl`. The irreps of $p31m'$ are very simple: the high symmetry momenta are Γ, K, and K' where all irreps are those of the point group 3, so irreps at $\phi = 0$ reduce to their C_3 eigenvalues at $\phi \neq 0$. We find

$$\mathcal{B}^{\phi=2\pi} = \mathcal{B}^{\phi=0} \downarrow p31m' = 2\Gamma_1 + K_2 + K_3 + K_2' + K_3' \tag{60}$$

where the irreps in $p31m'$ that appear in Eq. (60) are defined

$$\begin{array}{c|cc} 3m' & 1 & C_3 \\ \hline \Gamma_1 & 1 & 1 \end{array}, \quad \begin{array}{c|cc} 3 & 1 & C_3 \\ \hline K_2 & 1 & e^{\frac{2\pi i}{3}} \\ K_3 & 1 & e^{-\frac{2\pi i}{3}} \end{array}, \quad \begin{array}{c|cc} 3 & 1 & C_3 \\ \hline K_2' & 1 & e^{-\frac{2\pi i}{3}} \\ K_3' & 1 & e^{\frac{2\pi i}{3}} \end{array}. \tag{61}$$

As discussed, the particle-hole symmetry $\mathcal{P}$ ensures that the irreps at the K and K' points are degenerate, so $K_2 + K_3$ and $K_2' + K_3'$ should be thought of as co-irreps. We can induce $\mathcal{B}^{\phi=2\pi}$ from the elementary band representations of $p31m'$:

$$\mathcal{B}^{\phi=2\pi} = A_{2b} \uparrow p31m' \tag{62}$$

where $2b$ is the Wyckoff position consisting of the $M\mathcal{T}$-related corners of the moiré unit cell (the AB and BA positions shown in Fig. 9) and the two-dimensional A irrep is two s orbitals, i.e. the representation of C_3 is $\mathbb{1}_{2\times 2}$. From Eq. (62), we see that the band representation of TBG at 2π flux can be obtained from elementary band representations. This fact, coupled with the calculation of trivial Wilson loops, demonstrates the elementary band representation is not topological. Note that the unitary particle-hole symmetry P acts as inversion in real space, and is implemented on the A_{2b} irrep by exchanging the s orbitals at AB and BA sites. Because there is no obstruction to locally realizing all symmetries of TBG at 2π flux, lattice model approaches[81,82] can faithfully capture the the topology. However, although $\mathcal{B}^{\phi=2\pi}$ is an elementary band representation, the Bilbao crystallographic server reveals that it is decomposable into two topological bands with Chern numbers ± 1 if the particle-hole symmetry P is broken and the flat bands gap. This case is discussed in Ref.[33].

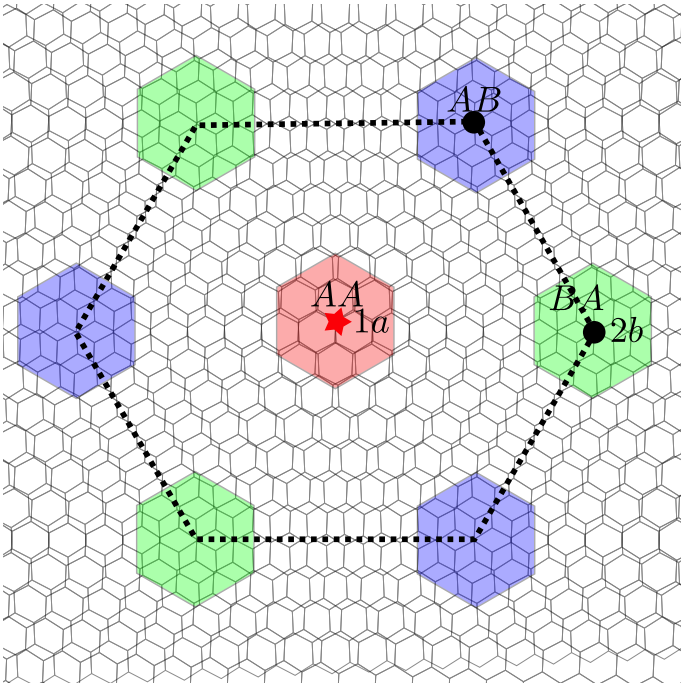

FIG. 9. Moiré lattice in real space, with colored regions denoting the AA and AB, BA stacking regions. The band representation $\mathcal{B}^{\phi=2\pi}$ can be induced from s orbitals at the 2b position, which is composed of the AB and BA moiré sites.

C. Chiral Anomaly in TBG

Ref.[83] first identified a special region in the TBG parameter space called the chiral limit where $w_0 = 0$ (w_1 is unrestricted). In the chiral limit, an anti-commuting symmetry $C = \tau_0 \otimes \sigma_3 \otimes \mathbb{1}$ (τ_0 is the 2×2 identity on the layer indices and $\mathbb{1}$ is the identity on the Landau level indices) appears which obeys

$$\{C, H_{BM}^{\phi}\} = 0 \tag{63}$$

for all flux ϕ. We see this from Eq. 228 of Ref.[38] because only σ_1 and σ_2 matrices appear when $w_0 = 0$ (see Ref.[38]). In zero flux, Ref.[83] identifies a discrete series of w_1 values where the two bands become *exactly* flat and have opposite chirality.

We now show that in chiral TBG at 2π flux, there are two exactly flat bands for *all* values of w_1, as we observe in Fig. 6(e). We will prove this is protected by the two flat bands having the *same* chirality. This is known as the chiral anomaly, which is a non-crystalline representation of chiral symmetry and cannot be realized in zero flux. First, recall that any state $|E\rangle$ at energy $E \neq 0$ yields a distinct state $|-E\rangle = C|E\rangle$ of energy $-E$, and the chiral eigenvalues on the basis $|E\rangle, |-E\rangle$ are ± 1 because

they are exchanged by C. We can determine the chiral eigenvalues of the flat bands in TBG analytically in the small w_1 limit where the kinetic term dominates and

$$H_{BM}^{\phi}(\mathbf{r}) \to \begin{pmatrix} v_F \boldsymbol{\sigma}\cdot\boldsymbol{\pi} & 0 \\ 0 & v_F \boldsymbol{\sigma}\cdot\boldsymbol{\pi} \end{pmatrix}, \quad \text{as } w_1 \to 0\ . \tag{64}$$

The eigenstates are in the form $(|E_n\rangle, \pm|E_n\rangle)^T$ where the $\pm$ states are orthogonal (so there are two states of energy E_n to account for the two layers) and the Dirac Hamiltonian eigenstates are defined

$$|E_0\rangle = \begin{pmatrix} |0\rangle \\ 0 \end{pmatrix}, \quad |E_n\rangle = \frac{1}{\sqrt{2}} \begin{pmatrix} ||n|\rangle \\ \mathrm{sgn}(n)\,||n|-1\rangle \end{pmatrix}, n \neq 0 \tag{65}$$

with energies $\boldsymbol{\sigma}\cdot\boldsymbol{\pi}\,|E_n\rangle = \mathrm{sgn}(n)\sqrt{2|n|\phi/\Omega}\,|E_n\rangle$ and $\mathrm{sgn}(0) = 0$. The chirality operator on the Dirac states obeys

$$\sigma_3\,|E_0\rangle = +\,|E_0\rangle\,, \quad \sigma_3\,|E_n\rangle = |E_{-n}\rangle\ . \tag{66}$$

In the $w_1 \to 0$ limit, the zero energy flat band eigenstates of H_{BM} in the chiral limit are

$$\frac{1}{\sqrt{\mathcal{N}(\mathbf{k})}} \sum_{\mathbf{R}} e^{-i\mathbf{k}\cdot\mathbf{R}} T_{\mathbf{a}_1}^{\mathbf{b}_1\cdot\mathbf{R}} T_{\mathbf{a}_2}^{\mathbf{b}_2\cdot\mathbf{R}} \begin{pmatrix} |E_0\rangle \\ \pm|E_0\rangle \end{pmatrix} \tag{67}$$

at every $\mathbf{k} \in BZ$. The bands in Eq. (67) carry chiral eigenvalues $+1, +1$. Note that the chiral eigenvalues protect the perfectly flat bands at all $\mathbf{k}$: if the energy of either of the flat bands states was not exactly zero, then $C\,|E\rangle$ would be a distinct state and the pair would have chiral eigenvalues ±1. Hence the $+1, +1$ eigenvalues pin the states to zero energy. We now show this is true for $w_1 \neq 0$. The proof is by contradiction. First, we increase w_1 away from zero so the flat band eigenstates are superpositions of many Landau levels. However, the chiral eigenvalues cannot change from $+1, +1$. All gap closings occur as states $|\pm E\rangle$ touch the zero energy flat bands, but a pair of states $|\pm E\rangle$ necessarily has chiral eigenvalues ±1 so the sum of the chiralities of the occupied bands is always 2. Thus two states are always pinned to zero energy at every $\mathbf{k}$ and all w_1, yielding exactly flat bands at *all* angles. We emphasize that this situation is very different than at zero flux where the chiral eigenvalues of the flat bands are ±1 which allows them to gap at generic values of w_1.

The $+1, +1$ chiral eigenvalues are called the chiral anomaly because the trace of C over all bands at fixed $\mathbf{k}$ formally satisfies

$$\begin{aligned} \mathrm{Tr}\ C &= \sum_{N=-\infty}^{\infty} U_N^{\dagger}(\mathbf{k})\sigma_3 U_N(\mathbf{k}) \\ &= \sum_{N=\pm1} U_N^{\dagger}(\mathbf{k})\sigma_3 U_N(\mathbf{k}) = 2 \end{aligned} \tag{68}$$

which is anomalous because $\mathrm{Tr}\ \sigma_3 = 0$. As in Eq. (45), $U_N(\mathbf{k})$ is the eigenvector of the Nth band at momentum $\mathbf{k}$. In the second line of Eq. (68), we used the ±1 chiral eigenvalues of states at $E \neq 0$ to cancel them from the sum, leaving only the passive bands. The fact that $\mathrm{Tr}\ C = 2$ can be understood from the Atiyah-Singer index theorem[84,85] which states that each Dirac Hamiltonian contributes $\phi/(2\pi)$ to the trace of the chirality operator, so $\mathrm{Tr}\ C = 2$ at $\phi = 2\pi$ because there are two layers[66]. Strictly speaking, we cannot apply the index theorem because we have constructed the spectrum on an infinite plane which is not compact. However, we can effectively compactify the spectrum by taking $\mathbf{k}$ to be discrete with L^2 values in the BZ corresponding to an $L\mathbf{a}_1 \times L\mathbf{a}_2$ torus in real space. Then there are a total of $2L^2$ zero modes of $+1$ chirality from Eq. (68), so $\mathrm{Tr}\ C = 2$ at each $\mathbf{k}$.

We can also consider the second chiral limit of TBG identified in Ref.[58] where $w_0 \neq 0$ and $w_1 = 0$. This limit has the chiral symmetry $C' = \tau_3\sigma_3$ where τ_3 is the Pauli matrix acting on the layer index. Numerically, we do not find zero-energy bands in the second chiral limit. This is because the Dirac zero modes in the top and bottom layers have opposite chiralities due to τ_3, so there is no chiral anomaly to protect the exact flatness.

IX. TWISTED BILAYER GRAPHENE: MANY-BODY PHYSICS

The rich single-particle physics of TBG at 2π flux, discussed at length in Sec. VIII, is characterized by the presence of low-energy flat bands. At the magic angle $\theta = 1.05$, the theoretically predicted small bandwidth $\sim$ 2meV means that the Coulomb interaction, which is $\sim$ 24meV, is the dominant term in the TBG Hamiltonian[86]. The large gap to the passive bands of $\sim$ 40meV makes a strong coupling approximation viable where the Coulomb Hamiltonian is projected into the flat bands and the flat band kinetic energy is neglected. This strategy has been used to great effect in predicting the groundstate properties of TBG near zero flux[56,57,86–89].

Because the kinetic band energy is $<$ 2meV and the Zeeman spin splitting is also $\sim$ 2meV at 30T, it is consistent to neglect both terms in the Hamiltonian at 2π flux. In this case, a $U(4)$ symmetry emerges in the strong coupling approximation just like at $\phi = 0$. Briefly, the spin and valley degeneracies act locally on the momentum $\mathbf{k}$ and lead to a $U(2) \times U(2)$ symmetry group, which is expanded in the strong coupling approximation to $U(4)$ by the operator $C_{2z}P$ which also acts locally on $\mathbf{k}$ (see Ref.[38]). Note that $C_{2z}P$ commutes with the Coulomb term in Eq. (42) but anti-commutes with the single-particle Hamiltonian H_0 which is why only the enhanced symmetry appears only in the strong coupling approximation where H_0 is set to zero in the flat bands. This is briefly reviewed in Ref.[38] and explained in depth in Ref.[86].

We now apply the results of Sec. VII to TBG, setting

the screened Coulomb interaction to

$$V(\mathbf{q}) = \pi\xi^2 U_\xi \frac{\tanh \xi|\mathbf{q}|/2}{\xi|\mathbf{q}|/2} \tag{69}$$

where the parameters of the screened Coulomb interaction are $\xi = 10$nm, $U_\xi = e^2/(\epsilon\xi) = 24$meV where ϵ is the dielectric constant[86].

A. Many-body Insulator Eigenstates

Because the flat bands, approximate spin rotation, and valley symmetry survive the addition of 2π flux, one may add Coulomb interactions in the same manner as TBG in zero flux: by projecting density-density terms into the 8 flat bands. These 8 bands have the creation operators $\gamma^\dagger_{\mathbf{k},M,\eta,s}$ where $M = \pm 1$ is the band, η is the valley, and s is the spin. We note that $\gamma^\dagger_{\mathbf{k}+2\pi\mathbf{G},M,\eta,s} = \gamma^\dagger_{\mathbf{k},M,\eta,s}$ because the eigenstates are periodic in $\mathbf{k}$ (see Sec. III B). Just as in zero-flux, the density-density form of the Coulomb interaction in Eq. (42) (that has neither spin nor valley dependence) takes the positive-semidefinite form

$$H_{int} = \frac{1}{2\Omega_{tot}} \sum_{\mathbf{q}\in BZ} \sum_{\mathbf{G}} O_{-\mathbf{q},-\mathbf{G}} O_{\mathbf{q},\mathbf{G}}, \tag{70}$$

where Ω_{tot} is the total area of the sample and the operators $O_{\mathbf{q},\mathbf{G}} = O^\dagger_{-\mathbf{q},-\mathbf{G}}$ are

$$O_{\mathbf{q},\mathbf{G}} = \sqrt{V(\mathbf{q}+2\pi\mathbf{G})} \sum_{\mathbf{k}\in BZ} \sum_{\eta,s} \sum_{MN} \bar{M}^\eta_{MN}(\mathbf{k}, \mathbf{q}+2\pi\mathbf{G}) \times (\gamma^\dagger_{\mathbf{k}-\mathbf{q},M,\eta,s}\gamma_{\mathbf{k},N,\eta,s} - \frac{1}{2}\delta_{MN}\delta_{\mathbf{q},0}) \ . \tag{71}$$

An expression for the form factor $\bar{M}^\eta_{MN}(\mathbf{k},\mathbf{q})$ is given in Eq. 282 of Ref.[38]. The term $\frac{1}{2}\delta_{MN}\delta_{\mathbf{q},0}$ is added to make H_{int} symmetric about charge neutrality as in Ref.[86]. To project in the flat bands, we merely restrict M, N to the flat bands which we label ± 1. If all flat band states of a given valley η and spin s are filled, $O_{\mathbf{q},\mathbf{G}}$ annihilates the state for all $\mathbf{q} \neq 0 \bmod 2\pi\mathbf{G}$. This allows for the construction of exact eigenstates at filling $\nu = -4, -2, 0, 2, 4$:

$$|\Psi_\nu\rangle = \prod_{\mathbf{k}} \prod_{j}^{(\nu+4)/2} \gamma^\dagger_{\mathbf{k},+,s_j,\eta_j} \gamma^\dagger_{\mathbf{k},-,s_j,\eta_j} |0\rangle \,, \tag{72}$$

where $\gamma^\dagger_{\mathbf{k},\pm,s_j,\eta_j}$ operators create flat band eigenstates with spin s_j and valley η_j which are arbitrary. Different choices of j are related by $U(4)$[56]. The states $|\Psi_\nu\rangle$ all have zero Chern number because the two flat bands have no total winding (see Sec. VIII A). The operators $O_{\mathbf{q}}$ act simply on these states as calculated in Ref.[38]:

$$O_{\mathbf{q},\mathbf{G}} |\Psi_\nu\rangle = \delta_{\mathbf{q},0} \lambda_{\mathbf{G}} |\Psi_\nu\rangle \tag{73}$$

where $\mathbf{q}$ here is restricted to the BZ and

$$\lambda_{\mathbf{G}} = \nu\sqrt{V(2\pi\mathbf{G})} \sum_{\mathbf{k}\in BZ} \frac{1}{2} \mathrm{Tr}\ \bar{M}(\mathbf{k}, 2\pi\mathbf{G}) \ . \tag{74}$$

We prove in Ref.[38] that $\bar{M}^\eta(\mathbf{k}, 2\pi\mathbf{G})$ and $\bar{M}^{-\eta}(\mathbf{k}, 2\pi\mathbf{G})$ are related by a unitary transform, so we drop the η label on quantities which are independent of valley, such as Tr $\bar{M}^\eta(\mathbf{k}, 2\pi\mathbf{G})$. Appealing to Eq. (70), we show in Ref.[38] that the energy of the eigenstates is

$$H_{int} |\Psi_\nu\rangle = \left(\frac{1}{2\Omega_{tot}} \sum_{\mathbf{G}} |\lambda_{\mathbf{G}}|^2 \right) |\Psi_\nu\rangle \tag{75}$$

which vanishes at the charge neutrality point $\nu = 0$ because $\lambda_{\mathbf{G}} \propto \nu$. Because H_{int} is positive semi-definite, $|\Psi_0\rangle$ must be a groundstate because it has zero energy at $\nu = 0$. Additionally, the $\nu = \pm 4$ eigenstates are trivially groundstates because they are fully filled/fully empty. Whether the $|\Psi_\nu\rangle$ are true groundstates for $\nu = \pm 2$ is still in question. One way to assess the groundstates at $\nu = 2$ is with the flat metric condition[58], which is the approximation

$$\bar{M}^\eta(\mathbf{k}, 2\pi\mathbf{G}) = m_{\mathbf{G}} \mathbb{1}_{2\times 2}, \tag{76}$$

in other words that $\bar{M}(\mathbf{k}, 2\pi\mathbf{G})$ is multiple of the identity matrix which does not depend on $\mathbf{k}$ at each $\mathbf{G}$. In Ref.[56] it was shown that if the flat metric condition is satisfied, then $|\Psi_\nu\rangle$ are necessarily groundstates. Ref.[38] contains a detailed review of this claim. In Fig. 10, we numerically calculate the singular values of $M(\mathbf{k}, 2\pi\mathbf{G})$ as in Ref.[56] and argue that Eq. (76) holds to a high degree of accuracy for all $2\pi|\mathbf{G}| \neq \sqrt{3}k_\theta$, as is also the case at $\phi = 0$. For six $\mathbf{G}$ momenta $\pm\mathbf{b}_1, \pm\mathbf{b}_2, \pm(\mathbf{b}_1 - \mathbf{b}_2)$ where $2\pi|\mathbf{G}| = \sqrt{3}k_\theta$, the flat metric condition is still an acceptable approximation to an accuracy in energy of $\Omega^{-1}V(2\pi\sqrt{3}k_\theta) \sim 10$meV times a numerical $O(1)$ constant depending on the violation of Eq. (76). From Eq. (10), the difference of the eigenvalues of $M^\dagger(\mathbf{k}, 2\pi\mathbf{G})M(\mathbf{k}, 2\pi\mathbf{G})$ is $\lesssim .33$, whereas if the flat metric condition held, the difference would be zero. Hence we estimate that the flat metric condition holds within $\Omega^{-1}V(2\pi\sqrt{3}k_\theta) \times \sqrt{.33} \sim 5$meV. Unless states other than $|\Psi_\nu\rangle$ are very competitive in energy, we can assume that $|\Psi_\nu\rangle$ is a groundstate at $\nu = \pm 2$. The excitation spectrum above these ground states at 2π flux is studied in Ref.[33]. Ref.[90] uses a complimentary technique to study the strong coupling excitations in small magnetic fields.

X. DISCUSSION

The techniques developed in this paper allow for an analysis of general periodic Hamiltonians in 2π flux — most notably the continuum models of moiré metamaterials — generalizing Bloch's theorem in a way that allows theoretical access to non-Peierls physics. We derived formulae for matrix elements, Wilson loops and

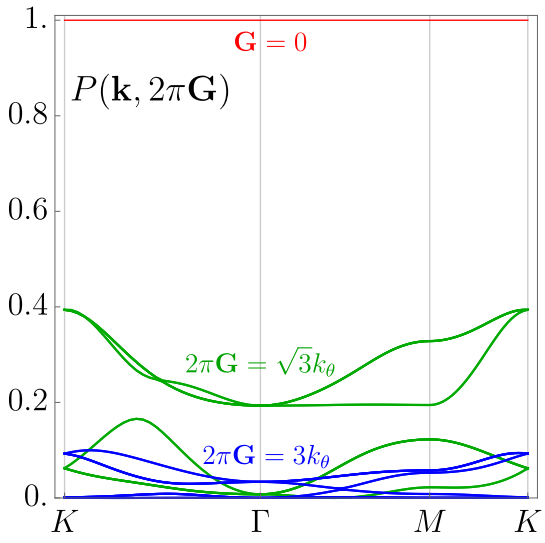

FIG. 10. The validity of the flat metric condition can be evaluated by examining the eigenvalues of $P(\mathbf{k}, 2\pi\mathbf{G}) = M^\dagger(\mathbf{k}, 2\pi\mathbf{G})M(\mathbf{k}, 2\pi\mathbf{G})$ as a function of $\mathbf{k}$. At $\mathbf{G} = 0$ (red), $M(\mathbf{k}, 0) = U^\dagger(\mathbf{k})U(\mathbf{k})$ is the identity matrix so the flat metric condition is exactly satisfied. Because the form factor $M(\mathbf{k}, 2\pi\mathbf{G})$ decays exponentially in $\mathbf{G}$, the flat metric condition is very nearly true for $|\mathbf{G}| \geq 3$ (blue) because the eigenvalues are quite small. Thus the validity of the flat metric condition is determined to very good approximation by only the first momentum shell composed of $\mathbf{G} = \pm\mathbf{b}_1, \pm\mathbf{b}_2, \pm(\mathbf{b}_1 - \mathbf{b}_2)$ (green). We see that, while $M(\mathbf{k}, 2\pi\mathbf{G})$ is not proportional to the identity, the differences between the eigenvalues of $P(\mathbf{k}, 2\pi\mathbf{G})$ are $\lesssim .33$ which is only a small violation of the flat metric condition. We used the parameters $\theta = 1.05$ and $w_0 = .8w_1$, but we checked that the flat metric condition is reliable over a range of parameters.

Berry curvature, and projected density-density interactions. These tools expand the reach of modern topological band theory to the strong flux limit, opening Hofstadter topology to analytical and numerical study in the continuum.

Using these techniques, we build a physical picture of twisted bilayer graphene in 2π flux — a tantalizing experimental setup as the large moiré unit cell allows for laboratory access to the Hofstadter limit for intermediate and large flux[34,91]. We find that in magic angle twisted bilayer graphene, the flat bands are reenter at 2π flux after splitting and broadening into Hofstadter bands at intermediate flux. The chiral limit of TBG, although physically inaccessible, showcases the chiral anomaly and exemplifies the non-crystalline properties of Hofstadter phases.

A natural development of this work is the extension of our gauge-invariant method to study the topology of band structures at general rational flux, which we pursue in future work. Such a development would be a powerful tool to study non-Peierls physics in topological magnetic systems, particularly with the ability to perform gauge-invariant Wilson loop calculations within our formalism. Investigations of strongly correlated phases like superconductivity and the fractional quantum hall effect are also made possible due to our expressions for the form factors.

During the preparation of this work, Ref.[92] independently studied the chiral limit in magnetic field. They find exact eigenstates for the zero-energy flat bands protected by chiral symmetry at *all* flux, but their techniques do not generalize to non-chiral Hamiltonians. We identify the same phase transition in Fig. 6(e) as described in their work.

XI. ACKNOWLEDGEMENTS

We thank Zhi-Da Song and Dmitri Efetov for their insight. B.A.B. and A.C. were supported by the ONR Grant No. N00014-20-1-2303, DOE Grant No. DESC0016239, the Schmidt Fund for Innovative Research, Simons Investigator Grant No. 404513, the Packard Foundation, the Gordon and Betty Moore Foundation through Grant No. GBMF8685 towards the Princeton theory program, and a Guggenheim Fellowship from the John Simon Guggenheim Memorial Foundation. Further support was provided by the NSF-MRSEC Grant No. DMR-1420541 and DMR-2011750, BSF Israel US foundation Grant No. 2018226, and the Princeton Global Network Funds. JHA is supported by a Marshall Scholarship funded by the Marshall Aid Commemoration Commission.

[1] Eva Y Andrei, Dmitri K Efetov, Pablo Jarillo-Herrero, Allan H MacDonald, Kin Fai Mak, T Senthil, Emanuel Tutuc, Ali Yazdani, and Andrea F Young. The marvels of moiré materials. *Nature Reviews Materials*, pages 1–6, 2021.

[2] Yuan Cao, Valla Fatemi, Ahmet Demir, Shiang Fang, Spencer L. Tomarken, Jason Y. Luo, Javier D. Sanchez-Yamagishi, Kenji Watanabe, Takashi Taniguchi, Efthimios Kaxiras, Ray C. Ashoori, and Pablo Jarillo-Herrero. Correlated insulator behaviour at half-filling in magic-angle graphene superlattices. *Nature (London)*, 556(7699):80–84, Apr 2018. doi:10.1038/nature26154.

[3] Yuan Cao, V. Fatemi, S. Fang, K. Watanabe, T. Taniguchi, E. Kaxiras, and P. Jarillo-Herrero. Unconventional superconductivity in magic-angle graphene superlattices. *Nature*, 556:43–50, 2018.

[4] Kyounghwan Kim, Ashley DaSilva, Shengqiang Huang, Babak Fallahazad, Stefano Larentis, Takashi Taniguchi, Kenji Watanabe, Brian J. LeRoy, Allan H. MacDonald, and Emanuel Tutuc. Tunable moiré bands and strong cor-

relations in small-twist-angle bilayer graphene. *Proceedings of the National Academy of Sciences*, 114(13):3364–3369, 2017. ISSN 0027-8424. doi:10.1073/pnas.1620140114. URL https://www.pnas.org/content/114/13/3364.

[5] Leon Balents, Cory R Dean, Dmitri K Efetov, and Andrea F Young. Superconductivity and strong correlations in moiré flat bands. *Nature Physics*, 16(7):725–733, 2020.

[6] Jianpeng Liu and Xi Dai. Orbital magnetic states in moiré graphene systems. *Nature Reviews Physics*, pages 1–16, 2021.

[7] Yanbang Chu, Le Liu, Yalong Yuan, Cheng Shen, Rong Yang, Dongxia Shi, Wei Yang, and Guangyu Zhang. A review of experimental advances in twisted graphene moiré superlattice. *Chinese Physics B*, 29(12):128104, dec 2020. doi:10.1088/1674-1056/abb221. URL https://doi.org/10.1088/1674-1056/abb221.

[8] Jiawei Zang, Jie Wang, Jennifer Cano, and Andrew J. Millis. Hartree-Fock Study of the Moiré Hubbard Model for Twisted Bilayer Transition Metal Dichalcogenides. *arXiv e-prints*, art. arXiv:2105.11883, May 2021.

[9] J. Zak. Magnetic translation group. *Phys. Rev.*, 134: A1602–A1606, Jun 1964. doi:10.1103/PhysRev.134.A1602. URL https://link.aps.org/doi/10.1103/PhysRev.134.A1602.

[10] Douglas R. Hofstadter. Energy levels and wave functions of bloch electrons in rational and irrational magnetic fields. *Phys. Rev. B*, 14:2239–2249, Sep 1976. doi:10.1103/PhysRevB.14.2239.

[11] C. Albrecht, J. H. Smet, K. von Klitzing, D. Weiss, V. Umansky, and H. Schweizer. Evidence of hofstadter's fractal energy spectrum in the quantized hall conductance. *Phys. Rev. Lett.*, 86:147–150, Jan 2001. doi:10.1103/PhysRevLett.86.147. URL https://link.aps.org/doi/10.1103/PhysRevLett.86.147.

[12] B. Hunt, J. D. Sanchez-Yamagishi, A. F. Young, M. Yankowitz, B. J. LeRoy, K. Watanabe, T. Taniguchi, P. Moon, M. Koshino, P. Jarillo-Herrero, and R. C. Ashoori. Massive dirac fermions and hofstadter butterfly in a van der waals heterostructure. *Science*, 340(6139):1427–1430, 2013. ISSN 0036-8075. doi:10.1126/science.1237240.

[13] C. R. Dean, L. Wang, P. Maher, C. Forsythe, F. Ghahari, Y. Gao, J. Katoch, M. Ishigami, P. Moon, M. Koshino, T. Taniguchi, K. Watanabe, K. L. Shepard, J. Hone, and P. Kim. Hofstadter's butterfly and the fractal quantum hall effect in moirésuperlattices. *Nature*, 497:598 EP –, 05 2013.

[14] Rafi Bistritzer and Allan H. MacDonald. Moiré bands in twisted double-layer graphene. *Proceedings of the National Academy of Science*, 108(30):12233–12237, Jul 2011. doi:10.1073/pnas.1108174108.

[15] J. Zak. Magnetic translation group. ii. irreducible representations. *Phys. Rev.*, 134:A1607–A1611, Jun 1964. doi:10.1103/PhysRev.134.A1607. URL https://link.aps.org/doi/10.1103/PhysRev.134.A1607.

[16] E. Brown. Aspects of group theory in electron dynamics**this work supported by the u.s. atomic energy commission. 22:313–408, 1969. ISSN 0081-1947. doi:https://doi.org/10.1016/S0081-1947(08)60033-8. URL https://www.sciencedirect.com/science/article/pii/S0081194708600338.

[17] P Streda. Theory of quantised hall conductivity in two dimensions. *Journal of Physics C: Solid State Physics*, 15(22):L717–L721, aug 1982. doi:10.1088/0022-3719/15/22/005. URL https://doi.org/10.1088/0022-3719/15/22/005.

[18] G. H. Wannier. A Result Not Dependent on Rationality for Bloch Electrons in a Magnetic Field. *Physica Status Solidi B Basic Research*, 88(2):757–765, August 1978. doi:10.1002/pssb.2220880243.

[19] J. Milton Pereira, F. M. Peeters, and P. Vasilopoulos. Landau levels and oscillator strength in a biased bilayer of graphene. *Phys. Rev. B*, 76:115419, Sep 2007. doi:10.1103/PhysRevB.76.115419. URL https://link.aps.org/doi/10.1103/PhysRevB.76.115419.

[20] Di Xiao, Ming-Che Chang, and Qian Niu. Berry phase effects on electronic properties. *Rev. Mod. Phys.*, 82:1959–2007, Jul 2010. doi:10.1103/RevModPhys.82.1959. URL https://link.aps.org/doi/10.1103/RevModPhys.82.1959.

[21] Godfrey Gumbs, Desiré Miessein, and Danhong Huang. Effect of magnetic modulation on bloch electrons on a two-dimensional square lattice. *Phys. Rev. B*, 52:14755–14760, Nov 1995. doi:10.1103/PhysRevB.52.14755. URL https://link.aps.org/doi/10.1103/PhysRevB.52.14755.

[22] R. Bistritzer and A. H. MacDonald. Moiré butterflies in twisted bilayer graphene. *Phys. Rev. B*, 84(3):035440, July 2011. doi:10.1103/PhysRevB.84.035440.

[23] Csaba Töke, Michael R Peterson, Gun Sang Jeon, and Jainendra K Jain. Fractional quantum hall effect in the second landau level: the importance of inter-composite-fermion interaction. *Physical Review B*, 72(12):125315, 2005.

[24] Martin Greiter. Landau level quantization on the sphere. *Phys. Rev. B*, 83(11):115129, March 2011. doi:10.1103/PhysRevB.83.115129.

[25] R. Bistritzer and A. H. MacDonald. Moiré butterflies in twisted bilayer graphene. *Phys. Rev. B*, 84:035440, Jul 2011. doi:10.1103/PhysRevB.84.035440. URL https://link.aps.org/doi/10.1103/PhysRevB.84.035440.

[26] Tong zhong Li, Ke lin Wang, and Jinlong Yang. Thermal properties of a two-dimensional electron gas under a one-dimensional periodic magnetic field. *Journal of Physics: Condensed Matter*, 9:9299–9313, 1997.

[27] J. A. Crosse, Naoto Nakatsuji, Mikito Koshino, and Pilkyung Moon. Hofstadter butterfly and the quantum hall effect in twisted double bilayer graphene. *Physical Review B*, 102(3), Jul 2020. ISSN 2469-9969. doi:10.1103/physrevb.102.035421. URL http://dx.doi.org/10.1103/PhysRevB.102.035421.

[28] Biao Lian, Fang Xie, and B. Andrei Bernevig. Open momentum space method for the Hofstadter butterfly and the quantized Lorentz susceptibility. *Phys. Rev. B*, 103(16): L161405, April 2021. doi:10.1103/PhysRevB.103.L161405.

[29] Daniela Pfannkuche and Rolf R. Gerhardts. Theory of magnetotransport in two-dimensional electron systems subjected to weak two-dimensional superlattice potentials. *Phys. Rev. B*, 46:12606–12626, Nov 1992. doi:10.1103/PhysRevB.46.12606. URL https://link.aps.org/doi/10.1103/PhysRevB.46.12606.

[30] Manisha Arora, Rashi Sachdeva, and Sankalpa Ghosh. Hofstadter butterflies in magnetically modulated graphene bilayer: An algebraic approach. *Physica E Low-Dimensional Systems and Nanostructures*, 142:115311, August 2022. doi:10.1016/j.physe.2022.115311.

[31] Gaurav Chaudhary, A. H. MacDonald, and M. R. Norman. Quantum Hall Superconductivity from Moir{é} Landau Levels. *arXiv e-prints*, art. arXiv:2105.01243, May 2021.

[32] Yuan Cao, Jeong Min Park, Kenji Watanabe, Takashi Taniguchi, and Pablo Jarillo-Herrero. Large Pauli Limit Violation and Reentrant Superconductivity in Magic-Angle Twisted Trilayer Graphene. *arXiv e-prints*, art. arXiv:2103.12083, March 2021.

[33] Jonah Herzog-Arbeitman, Aaron Chew, Dmitri K Efetov, and B Andrei Bernevig. Reentrant correlated insulators in twisted bilayer graphene at 25 t (2 π flux). *Physical Review Letters*, 129(7):076401, 2022.

[34] Ipsita Das, Cheng Shen, Alexandre Jaoui, Jonah Herzog-Arbeitman, Aaron Chew, Chang-Woo Cho, Kenji Watanabe, Takashi Taniguchi, Benjamin A. Piot, B. Andrei Bernevig, and Dmitri K. Efetov. Observation of reentrant correlated insulators and interaction-driven fermi-surface reconstructions at one magnetic flux quantum per moiré unit cell in magic-angle twisted bilayer graphene. *Phys. Rev. Lett.*, 128:217701, May 2022. doi: 10.1103/PhysRevLett.128.217701. URL `https://link.aps.org/doi/10.1103/PhysRevLett.128.217701`.

[35] DLMF, Siegel Theta. *NIST Digital Library of Mathematical Functions*. http://dlmf.nist.gov/, Release 1.1.1 of 2021-03-15. URL `http://dlmf.nist.gov/21`. B. Deconinck.

[36] Robert C Gunning. *Riemann Surfaces and Generalized Theta Functions*, volume 91 of *Ergebnisse der Mathematik und ihrer Grenzgebiete. 2. Folge, A Series of Modern Surveys in Mathematics*. Springer Berlin Heidelberg, Berlin, Heidelberg, 1976. ISBN 3642663842.

[37] Alexander Maloney and Edward Witten. Averaging over Narain moduli space. *Journal of High Energy Physics*, 2020 (10):187, October 2020. doi:10.1007/JHEP10(2020)187.

[38] See supplementary materials for a description of additional calculations.

[39] Jennifer Cano, Barry Bradlyn, Zhijun Wang, L. Elcoro, M. G. Vergniory, C. Felser, M. I. Aroyo, and B. Andrei Bernevig. Topology of Disconnected Elementary Band Representations. *Phys. Rev. Lett.*, 120(26):266401, June 2018. doi:10.1103/PhysRevLett.120.266401.

[40] R. Peierls. Zur Theorie des Diamagnetismus von Leitungselektronen. *Zeitschrift fur Physik*, 80:763–791, November 1933. doi:10.1007/BF01342591.

[41] Jonah Herzog-Arbeitman, Zhi-Da Song, Nicolas Regnault, and B. Andrei Bernevig. Hofstadter topology: Noncrystalline topological materials at high flux. *Phys. Rev. Lett.*, 125:236804, Dec 2020. doi: 10.1103/PhysRevLett.125.236804. URL `https://link.aps.org/doi/10.1103/PhysRevLett.125.236804`.

[42] Sun-Woo Kim, Sunam Jeon, Moon Jip Park, and Youngkuk Kim. Replica Higher-Order Topology of Hofstadter Butterflies in Twisted Bilayer Graphene. *arXiv e-prints*, art. arXiv:2204.08087, April 2022.

[43] Yifei Guan, Oleg V. Yazyev, and Alexander Kruchkov. Re-entrant magic-angle phenomena in twisted bilayer graphene in integer magnetic fluxes. *arXiv e-prints*, art. arXiv:2201.13062, January 2022.

[44] Note1. In applications to TBG, $\mathbf{a}_i$ will be moiré lattice vectors.

[45] Nicola Marzari, Arash A. Mostofi, Jonathan R. Yates, Ivo Souza, and David Vanderbilt. Maximally localized Wannier functions: Theory and applications. *Reviews of Modern Physics*, 84(4):1419–1475, October 2012. doi: 10.1103/RevModPhys.84.1419.

[46] Note2. One can also construct states on a finite lattice in the same way. However, in this case one cannot perform the normalization sum in Eq. (18) analytically. Hence we only focus on the infinite case in this work.

[47] Note3. In the symmetric gauge, it is well known[93,94] that $\psi_0(\mathbf{r}) \sim \exp(-\phi\frac{r^2}{4\Omega}) = \exp(-|z|^2/4\ell_B^2)$ where $z = x + iy$ is the holomorphic coordinate and $\ell_B = 1/\sqrt{eB}$ is the magnetic length.

[48] Note4. The Siegel theta function, also known as the Riemann theta function, is implemented in Mathematica.

[49] D. J. Thouless, M. Kohmoto, M. P. Nightingale, and M. den Nijs. Quantized hall conductance in a two-dimensional periodic potential. *Phys. Rev. Lett.*, 49:405–408, Aug 1982. doi:10.1103/PhysRevLett.49.405.

[50] Jie Wang, Jennifer Cano, Andrew J. Millis, Zhao Liu, and Bo Yang. Exact Landau Level Description of Geometry and Interaction in a Flatband. *arXiv e-prints*, art. arXiv:2105.07491, May 2021.

[51] Note5. In many texts, the sign of the Chern number is made positive by orienting the B field in the $-\hat{z}$ direction. This is just a matter of convention.

[52] Christian Brouder, Gianluca Panati, Matteo Calandra, Christophe Mourougane, and Nicola Marzari. Exponential localization of wannier functions in insulators. *Physical Review Letters*, 98(4), Jan 2007. ISSN 1079-7114. doi: 10.1103/physrevlett.98.046402.

[53] Leticia Tarruell, Daniel Greif, Thomas Uehlinger, Gregor Jotzu, and Tilman Esslinger. Creating, moving and merging Dirac points with a Fermi gas in a tunable honeycomb lattice. *Nature (London)*, 483(7389):302–305, March 2012. doi:10.1038/nature10871.

[54] F. Yılmaz, F. Nur Ünal, and M. Ã. . Oktel. Evolution of the Hofstadter butterfly in a tunable optical lattice. *Phys. Rev. A*, 91(6):063628, June 2015. doi: 10.1103/PhysRevA.91.063628.

[55] M. Aidelsburger, M. Atala, M. Lohse, J. T. Barreiro, B. Paredes, and I. Bloch. Realization of the hofstadter hamiltonian with ultracold atoms in optical lattices. *Phys. Rev. Lett.*, 111:185301, Oct 2013. doi: 10.1103/PhysRevLett.111.185301. URL `https://link.aps.org/doi/10.1103/PhysRevLett.111.185301`.

[56] Biao Lian, Zhi-Da Song, Nicolas Regnault, Dmitri K. Efetov, Ali Yazdani, and B. Andrei Bernevig. Twisted bilayer graphene. IV. Exact insulator ground states and phase diagram. *Phys. Rev. B*, 103(20):205414, May 2021. doi: 10.1103/PhysRevB.103.205414.

[57] B. Andrei Bernevig, Biao Lian, Aditya Cowsik, Fang Xie, Nicolas Regnault, and Zhi-Da Song. Twisted bilayer graphene. V. Exact analytic many-body excitations in Coulomb Hamiltonians: Charge gap, Goldstone modes, and absence of Cooper pairing. *Phys. Rev. B*, 103(20): 205415, May 2021. doi:10.1103/PhysRevB.103.205415.

[58] B. Andrei Bernevig, Zhi-Da Song, Nicolas Regnault, and Biao Lian. Twisted bilayer graphene. I. Matrix elements, approximations, perturbation theory, and a k .p two-band model. *Phys. Rev. B*, 103(20):205411, May 2021. doi: 10.1103/PhysRevB.103.205411.

[59] Liujun Zou, Hoi Chun Po, Ashvin Vishwanath, and T. Senthil. Band structure of twisted bilayer graphene: Emergent symmetries, commensurate approximants, and wannier obstructions. *Phys. Rev. B*, 98:085435, Aug 2018. doi:10.1103/PhysRevB.98.085435. URL `https://link.aps.org/doi/10.1103/PhysRevB.98.085435`.

[60] Zhida Song, Zhijun Wang, Wujun Shi, Gang Li, Chen Fang, and B. Andrei Bernevig. All magic angles in twisted bilayer graphene are topological. *Physical Re-*

view Letters, 123(3), Jul 2019. ISSN 1079-7114. doi: 10.1103/physrevlett.123.036401. URL http://dx.doi.org/10.1103/PhysRevLett.123.036401.

[61] Eduardo Fradkin. *Quantum Field Theory: An Integrated Approach*. Princeton University Press, 2021.

[62] Michael Peskin. *An introduction to quantum field theory*. CRC press, 2018.

[63] Stephen L. Adler. Axial-vector vertex in spinor electrodynamics. *Phys. Rev.*, 177:2426–2438, Jan 1969. doi: 10.1103/PhysRev.177.2426. URL https://link.aps.org/doi/10.1103/PhysRev.177.2426.

[64] John S Bell and Roman Jackiw. A pcac puzzle: π 0 $\gamma\gamma$ in the σ-model. *Il Nuovo Cimento A (1965-1970)*, 60(1): 47–61, 1969.

[65] K. Fujikawa and H. Suzuki. *Path integrals and quantum anomalies*. 2004. doi: 10.1093/acprof:oso/9780198529132.001.0001.

[66] Matthew F. Lapa. Parity anomaly from the Hamiltonian point of view. *Phys. Rev. B*, 99(23):235144, June 2019. doi:10.1103/PhysRevB.99.235144.

[67] A. J. Niemi and G. W. Semenoff. Fermion Number Fractionization in Quantum Field Theory. *Phys. Rept.*, 135:99, 1986. doi:10.1016/0370-1573(86)90167-5.

[68] Edward Witten. The "parity" anomaly on an unorientable manifold. *Phys. Rev. B*, 94:195150, Nov 2016. doi: 10.1103/PhysRevB.94.195150. URL https://link.aps.org/doi/10.1103/PhysRevB.94.195150.

[69] Xiao-Liang Qi and Shou-Cheng Zhang. Topological insulators and superconductors. *Rev. Mod. Phys.*, 83:1057–1110, Oct 2011. doi:10.1103/RevModPhys.83.1057. URL https://link.aps.org/doi/10.1103/RevModPhys.83.1057.

[70] Note6. See Ref.[38] for a discussion of V_1 in the K' valley.

[71] Barry Bradlyn, Zhijun Wang, Jennifer Cano, and B. Andrei Bernevig. Disconnected elementary band representations, fragile topology, and wilson loops as topological indices: An example on the triangular lattice. *Physical Review B*, 99(4), Jan 2019. ISSN 2469-9969. doi: 10.1103/physrevb.99.045140. URL http://dx.doi.org/10.1103/PhysRevB.99.045140.

[72] Zhi-Da Song, Biao Lian, Nicolas Regnault, and B. Andrei Bernevig. Twisted bilayer graphene. ii. stable symmetry anomaly. *Physical Review B*, 103(20), May 2021. ISSN 2469-9969. doi:10.1103/physrevb.103.205412. URL http://dx.doi.org/10.1103/PhysRevB.103.205412.

[73] Adrien Bouhon, Annica M. Black-Schaffer, and Robert-Jan Slager. Wilson loop approach to fragile topology of split elementary band representations and topological crystalline insulators with time-reversal symmetry. *Phys. Rev. B*, 100(19):195135, November 2019. doi: 10.1103/PhysRevB.100.195135.

[74] Barry Bradlyn, L. Elcoro, Jennifer Cano, M. G. Vergniory, Zhijun Wang, C. Felser, M. I. Aroyo, and B. Andrei Bernevig. Topological quantum chemistry. *Nature (London)*, 547(7663):298–305, Jul 2017. doi: 10.1038/nature23268.

[75] Jennifer Cano, Barry Bradlyn, Zhijun Wang, L. Elcoro, M. G. Vergniory, C. Felser, M. I. Aroyo, and B. Andrei Bernevig. Building blocks of topological quantum chemistry: Elementary band representations. *Phys. Rev. B*, 97 (3):035139, Jan 2018. doi:10.1103/PhysRevB.97.035139.

[76] Note7. Technically $p6'2'2$ is a 3D space group. We only consider the $k_z = 0$ plane, which is equivalent to the 2D wallpaper group $p6'm'm$ because the action of M_y and C_{2x} is identical in 2D.

[77] Luis Elcoro, Benjamin J. Wieder, Zhida Song, Yuanfeng Xu, Barry Bradlyn, and B. Andrei Bernevig. Magnetic Topological Quantum Chemistry. *arXiv e-prints*, art. arXiv:2010.00598, October 2020.

[78] Ipsita Das, Xiaobo Lu, Jonah Herzog-Arbeitman, Zhi-Da Song, Kenji Watanabe, Takashi Taniguchi, B. Andrei Bernevig, and Dmitri K. Efetov. Symmetry-broken Chern insulators and Rashba-like Landau-level crossings in magic-angle bilayer graphene. *Nature Physics*, 17(6): 710–714, January 2021. doi:10.1038/s41567-021-01186-3.

[79] MI Aroyo, JM Perez-Mato, Cesar Capillas, Eli Kroumova, Svetoslav Ivantchev, Gotzon Madariaga, Asen Kirov, and Hans Wondratschek. Bilbao crystallographic server: I. databases and crystallographic computing programs. *ZEITSCHRIFT FUR KRISTALLOGRAPHIE*, 221:15–27, 01 2006. doi:10.1524/zkri.2006.221.1.15.

[80] Mois I. Aroyo, Asen Kirov, Cesar Capillas, J. M. Perez-Mato, and Hans Wondratschek. Bilbao Crystallographic Server. II. Representations of crystallographic point groups and space groups. *Acta Crystallographica Section A*, 62(2): 115–128, Mar 2006. doi:10.1107/S0108767305040286.

[81] Oskar Vafek and Jian Kang. Lattice model for the Coulomb interacting chiral limit of the magic angle twisted bilayer graphene: symmetries, obstructions and excitations. *arXiv e-prints*, art. arXiv:2106.05670, June 2021.

[82] Jian Kang and Oskar Vafek. Symmetry, maximally localized wannier states, and a low-energy model for twisted bilayer graphene narrow bands. *Phys. Rev. X*, 8:031088, Sep 2018. doi:10.1103/PhysRevX.8.031088. URL https://link.aps.org/doi/10.1103/PhysRevX.8.031088.

[83] Grigory Tarnopolsky, Alex Jura Kruchkov, and Ashvin Vishwanath. Origin of magic angles in twisted bilayer graphene. *Phys. Rev. Lett.*, 122:106405, Mar 2019. doi: 10.1103/PhysRevLett.122.106405. URL https://link.aps.org/doi/10.1103/PhysRevLett.122.106405.

[84] Michael Francis Atiyah and Isadore Manuel Singer. The index of elliptic operators: I. *Annals of mathematics*, pages 484–530, 1968.

[85] Tohru Eguchi, Peter B Gilkey, and Andrew J Hanson. Gravitation, gauge theories and differential geometry. *Physics reports*, 66(6):213–393, 1980.

[86] B. Andrei Bernevig, Zhi-Da Song, Nicolas Regnault, and Biao Lian. Twisted bilayer graphene. III. Interacting Hamiltonian and exact symmetries. *Phys. Rev. B*, 103(20): 205413, May 2021. doi:10.1103/PhysRevB.103.205413.

[87] Jian Kang and Oskar Vafek. Strong coupling phases of partially filled twisted bilayer graphene narrow bands. *Phys. Rev. Lett.*, 122:246401, Jun 2019. doi: 10.1103/PhysRevLett.122.246401. URL https://link.aps.org/doi/10.1103/PhysRevLett.122.246401.

[88] Jian Kang, B. Andrei Bernevig, and Oskar Vafek. Cascades between light and heavy fermions in the normal state of magic angle twisted bilayer graphene. *arXiv e-prints*, art. arXiv:2104.01145, April 2021.

[89] Patrick J. Ledwith, Eslam Khalaf, and Ashvin Vishwanath. Strong Coupling Theory of Magic-Angle Graphene: A Pedagogical Introduction. *arXiv e-prints*, art. arXiv:2105.08858, May 2021.

[90] Xiaoyu Wang and Oskar Vafek. Narrow bands in magnetic field and strong-coupling Hofstadter spectra. *arXiv e-prints*, art. arXiv:2112.08620, December 2021.

[91] Jiachen Yu, Benjamin A. Foutty, Zhaoyu Han, Mark E. Barber, Yoni Schattner, Kenji Watanabe, Takashi Taniguchi, Philip Phillips, Zhi-Xun Shen, Steven A. Kivel-

son, and Benjamin E. Feldman. Correlated Hofstadter Spectrum and Flavor Phase Diagram in Magic Angle Graphene. *arXiv e-prints*, art. arXiv:2108.00009, July 2021.

[92] Yarden Sheffer and Ady Stern. Chiral Magic-Angle Twisted Bilayer Graphene in a Magnetic Field: Landau Level Correspondence, Exact Wavefunctions and Fractional Chern Insulators. *arXiv e-prints*, art. arXiv:2106.10650, June 2021.

[93] S. M. Girvin. Course 2: The Quantum Hall Effect: Novel Excitations and Broken Symmetries. In A. Comtet, T. Jolicoeur, S. Ouvry, and F. David, editors, *Topological Aspects of Low Dimensional Systems*, volume 69, page 53, January 1999.

[94] Eduardo Fradkin. *Field Theories of Condensed Matter Physics*. Cambridge University Press, 2 edition, 2013. doi: 10.1017/CBO9781139015509.